SUPPORTING INFORMATION

Switching from Separated to Contact Ion-Pair Binding Modes with Diastereomeric Calix[4]pyrrole Bis-phosphonate Receptors

Moira Ciardi,[†] Francesca Tancini,[§] Guzmán Gil-Ramírez,[†] Eduardo C. Escudero Adán,[†] Chiara Massera,[§] Enrico Dalcanale,*[,§] and Pablo Ballester*[,†,‡]

†Institute of Chemical Research of Catalonia (ICIQ), Avda. Països Catalans 16, 43007 Tarragona, Spain

§Dipartimento di Chimica and Unità INSTM, UdR Parma, Università degli Studi di Parma, Parco Area delle Scienze 17/a, 43124 Parma, Italy

‡Catalan Institution of Research and Advanced Studies (ICREA), Passeig Lluís Companys 23, 08018 Barcelona, Spain

Table of Contents

1. General information and instrumentation.

All syntheses were carried out using chemicals as purchased from commercial sources unless otherwise noted. When required, dried and deoxygenated solvents supplied by Sigma-Aldrich Solvent Purification System (SPS-200-6) were used. Thin-layer chromatography (TLC) and flash column chromatography were performed with DC-Alufolien Kieselgel 60 F254 (Merck) and silica gel 60A for chromatography (SDS) respectively.

^{1}H and ^{31}P NMR spectra were recorded on a Bruker Avance 400 (400.1 MHz for ^{1}H NMR) and Bruker Avance 500 (500.1 MHz for ^{1}H NMR) ultrashield spectrometer; Mass Spectrometry experiments on a LCT Premier, Waters-Micromass ESI or Autoflex, Bruker Daltonics MALDI. FT-IR measurements were carried out on a Bruker Optics FTIR Alpha spectrometer equipped with a DTGS detector, KBr beam splitter at 4 cm^{-1} resolution. Isothermal titration calorimetry experiments (ITC) were performed using a Microcal VP-ITC Microcalorimeter. The conductimetric titrations were performed by Mettler-Toledo conductimeter, using a 84μS/cm sensor previously calibrated with a 0.00056 M KCl solution.

The conductimetric titrations were performed in 25 mL vials equipped with a magnetic stirring bar and placed on top of a stirring plate. The conductivity of a pure acetonitrile solution afforded a value of 0.22μS/cm. A solution of [TBACl] = 0.98 x 10^{-4} M in acetonitrile gave a conductivity value of 15.49 μS/cm. We placed 20 mL of the above solution in the 25 mL vial and added incremental amounts of a [**4oo]** = 1.7 x 10^{-3} M solution in the same solvent. After each addition the mixture was stirred for 2 minutes to ensure a good mixing of all the components. The measurement of the conductance of the solution was performed after switching off stirring. The process of stirring and measurement was repeated until a constant value for the conductance was obtained.

2. Synthetic Procedures.

Synthetic procedures used in the preparation of tetraol **1a**, *bis*-phosphonate cavitands **4**, bis-methylene cavitand **5,** aryl-extended calix[4]pyrrole **6** and their corresponding characterization data.

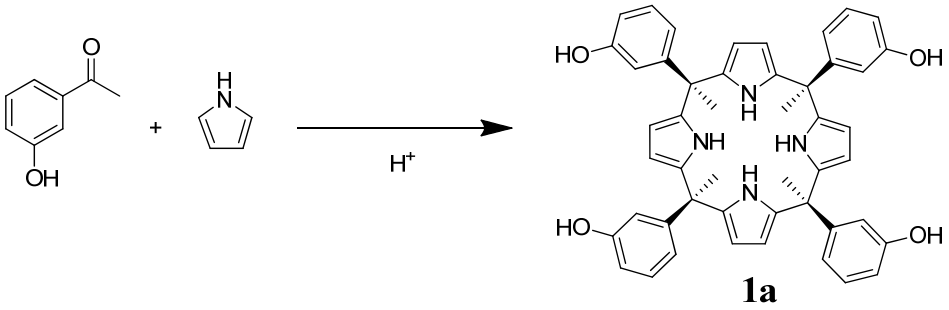

1a

Scheme S1. Synthetic scheme for the preparation of the tetraol precursor **1a**.

2.1.*meso*-Tetramethyltetrakis(hydroxyphenyl) calix[4]pyrrole **1a**[1]:

3-hydroxy acetophenone (6.0 g, 44mmol) was dissolved in HPLC grade MeOH (200 mL) and methanesulfonic acid was added dropwise (1.4 mL, 22.03mmol). The solution turned from pale yellow to red after addition of freshly distilled pyrrole (3 mL, 44mmol). The reaction was protected from light and refluxed for 3 hrs. Then quenched by addition of triethylamine (4 mL) and distilled water (200 mL). MeOH was evaporated and the aqueous solution extracted with AcOEt (3 × 200 mL). The collected organic fractions were dried over sodium sulphate and the solvent removed under reduced pressure. The desired isomer was filtered off by crystallization of the reaction crude from CH_3CN (20 mL) as white powder with a yield of 2%. ^{1}H-NMR (400 MHz, CD_3CN) δ_H ppm 7.96 (bs, 4H), 7.10 (t, 4H), 6.58 (dd, 4H), 6.51 (dd, 4H), 6.42 (bt, 4H), 6.04 (d, 8H), 2.15 (bs, 4H), 1.88 (s, 12H).

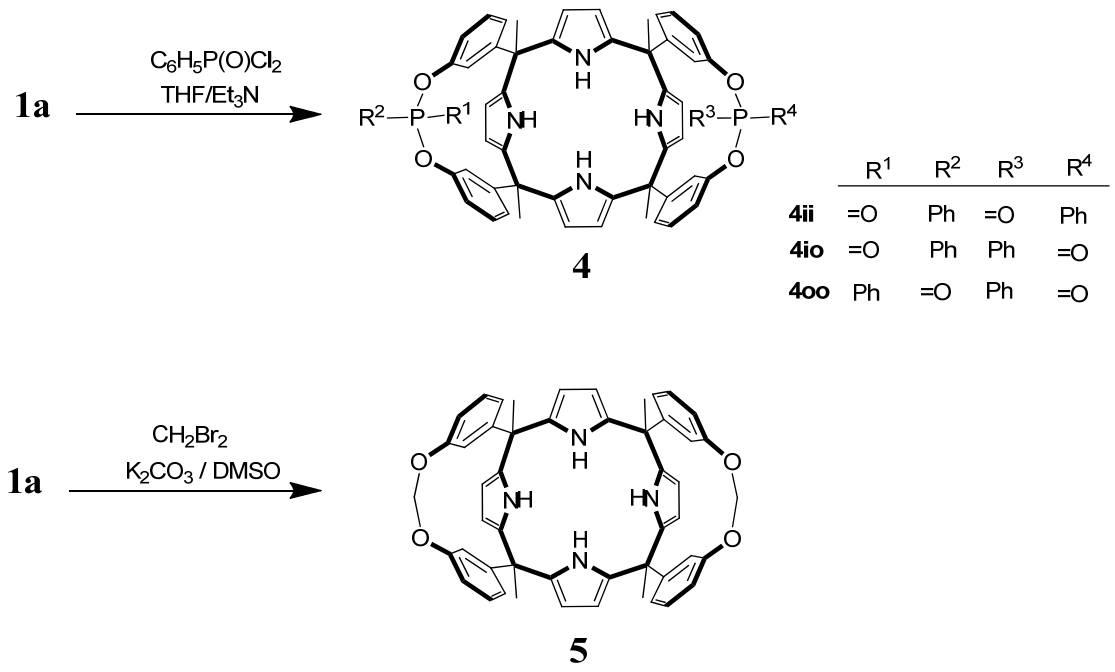

Scheme S2. Synthetic schemes for the preparations of **4** and **5** from precursor **1a**.

2.2. Bis-phosphonate cavitands **4**.

To a solution of calix[4]pyrrole **1a** (200 mg, 0.270mmol) in dry THF (10 mL) and freshly distilled triethylamine (0.753 mL, 5.40 mmol), phenylphosphonic dichloride (0.095 mL, 0.675 mmol) was added dropwise under argon atmosphere. The reaction mixture was stirred for 2 hrs at room temperature. The solvent was removed *in vacuo* and water (50 mL) was added to solubilise the triethylammonium chloride salt. The suspension was extracted with CH_2Cl_2 (2 × 50 mL). The organic extracts were combined, dried, filtered and the solvent removed *in vacuo*. The ^{1}H-NMR spectrum of the residue indicated the presence of a mixture of three diastereoisomers **4io, 4oo**, **4ii**. The reaction crude was first purified by Combiflash (SiO_2; CH_2Cl_2 : MeOH 99:1) in order to remove the oligomers/polymers formed during the reaction with 60% overall yield. The fraction containing the three diastereomers was purified by semipreparative HPLC (Spherisorb silica 250 × 20 mm, 5 μm; SiO_2; CH_2Cl_2 : MeOH 99:1) to yield each separated isomer **4io, 4oo** and **4ii** as a white solid (Retention times: 4.8 minutes, 6.19 minutes and 9.8 minutes, respectively). The isomers can be further purified by crystallization from acetonitrile.

We also conducted additional experiments towards the stereoselective preparation of phosphonate cavitand **4ii** following an alternative two-step procedure already applied in

the preparation of phosphonate resorcinarenes.[2] First, α,α,α,α-**1a** was reacted for 3 hrs at 70 ºC with dichloro(phenyl)phosphine using freshly distilled pyridine as solvent. The obtained phenyl-phosphonito intermediate was oxidized "in situ" by addition of a 35% solution of hydrogen peroxide to give the corresponding bis-phosphonate cavitands. Disappointingly, in this case the two step synthetic strategy turned out not to be stereoselective. The isolation of the isomers of **4** from that mixture was tedious and very time consuming. In addition, we detected in the reaction crude the presence of thermodynamically highly stable inclusion complexes of pyridine-*N*-oxide with the diastereomers of **4**. These inclusion complexes even survived column chromatography. Single crystals of the pyridine-*N*-oxide inclusion complex with **4io** suitable for X-ray diffraction grew from acetonitrile solution (Figure S1). The pyridine-*N*-oxide must have been produced during the oxidation of the phenyl-phosphonito cavitands, because we used pyridine as solvent in the first synthetic step. Additional efforts to optimize the two step reaction conditions (mildly oxidative conditions, use of a bulkier base like 2,6-dimethyl pyridine, addition of a co-solvent) were not successful.

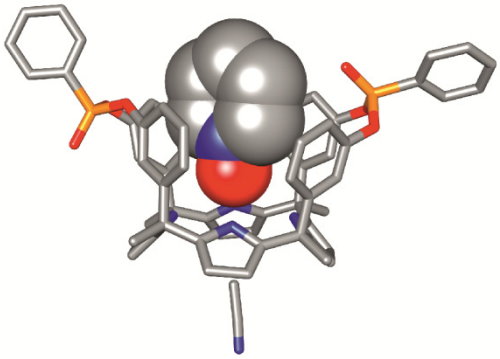

Figure S1. Solid state structure of the inclusion complex of pyridine-*N*-oxide (shown in CPK) with the phosphonate stereoisomer **4io**. The inclusion of the *N*-oxide in the deep aromatic cavity induces the receptor to adopt the cone conformation.

Experimental data for **4io** (white powder, 30%). M.p.: T > 200ºC (slow decomposition); ^{1}H-NMR (500 MHz, CD_2Cl_2, 25°C): δ (ppm) = 8.20 (bs, 1H), 8.08 (bs, 2H), 8.02 (m, $^{3}J_{H\text{-}P}$ ~ 14 Hz, $^{3}J_{H\text{-}H}$ ~ 7.3 Hz, $^{4}J_{H\text{-}H}$ ~ 1.2 Hz, 4H), 7.84 (bs, 1H), 7.71 (m, $^{3}J_{H\text{-}H}$ ~ 7.3 Hz, $^{4}J_{H\text{-}H} \approx {}^{5}J_{H\text{-}P}$ ~ 1.2 Hz, 2H), 7.61 (m, $^{3}J_{H\text{-}H}$ ~ 7.3 Hz, $^{4}J_{H\text{-}P}$ ~ 4.8 Hz, 4H), 7.32 (s, 2H), 7.25 (t, $^{3}J_{H\text{-}H}$ ~ 7.98 Hz, 2H), 7.21 (t, $^{3}J_{H\text{-}H}$ ~ 7.98 Hz, 2H), 7.02 (d, $^{3}J_{H\text{-}H}$ ~ 7.98 Hz, 2H), 7.01 (d, $^{3}J_{H\text{-}H}$ ~ 7.98 Hz, 2H), 7.00 (d, $^{3}J_{H\text{-}H}$ ~ 7.98 Hz, 2H), 6.95 (s, 2H), 6.83 (d, $^{3}J_{H\text{-}H}$ ~ 7.98 Hz, 2H), 6.23 (d, $^{4}J_{H\text{-}H}$ ~ 2.17 Hz, 2H), 6.2 (d, $^{4}J_{H\text{-}H}$ ~ 2.17 Hz, 2H), 5.96 (t, $^{4}J_{H\text{-}H} \approx {}^{3}J_{H\text{-}H}$ ~ 2.17 Hz, 2H), 5.91 (t, $^{4}J_{H\text{-}H} \approx {}^{3}J_{H\text{-}H}$ ~ 2.17 Hz, 2H), 2.02 (s, 6H), 2.0 (s, 6H). ^{31}P-NMR (500 MHz, CD_2Cl_2, 25°C): δ = (ppm) 15.53 (P(O)in), 13.27 (P(O)out). HR-

MALDI-MS: *m/z* calculated for $C_{60}H_{50}N_4O_6P_2$ 984.32, found 984.31; FT-IR ν (cm^{-1}) 3000 (P-CH_{Ar} streaching, 1580 (P-Ar aromatic ring in-plane stretching), 1480-1427 (P-Ar aromatic ring in-plane stretching), 1265,1228,1202 PO stretching; 942 (interaction between aromatic ring vibration and P-C stretching); elemental analysis calculated for $C_{60}H_{50}N_4O_6P_2$ + (3 × CH_3OH) (%): C, 69.99; H, 5.78; N, 5.18; found: C, 69.82; H, 5.34; N, 5.81.

Experimental data for **4oo** (white powder, 10%). M.p.: T > 180 ºC (slow decomposition); ^{1}H-NMR (500 MHz, CD_2Cl_2, 25°C): δ (ppm) = 8.04 (bs, 2H), 8.00 (m, $^3J_{H-P}$ ~ 14 Hz, $^3J_{H-H}$ ~ 7.3 Hz, $^4J_{H-H}$ ~ 1.2 Hz, 4H), 7.70 (m, $^3J_{H-H}$ ~ 7.3 Hz, $^4J_{H-H} \approx {}^5J_{H-P}$ ~ 1.2 Hz, 2H), 7.60 (m, $^3J_{H-H}$ ~ 7.3 Hz, $^4J_{H-P}$ ~ 4.8 Hz, 4H), 7.49 (bs, 2H), 7.26 (t, $^3J_{H-H}$ ~ 7.7 Hz, 4H), 7.22 (d, $^3J_{H-H}$ ~ 7.7 Hz, 4H), 7.18 (s, 4H), 6.86 (d, $^3J_{H-H}$ ~ 7.7 Hz, 4H), 6.32 (d, $^4J_{H-H}$ ~ 2.65 Hz, 4H), 5.50 (bs, 4H), 2.07 (s, 12H); ^{31}P-NMR (500 MHz, CD_2Cl_2, 25°C): δ (ppm) = 12.5; HR-MALDI-MS: m/z calculated for $C_{60}H_{50}N_4O_6P_2$ 984.32, found 984.3; FT-IR ν (cm^{-1}) 3000 (P-CH_{Ar} stretching), 1580 and 1480-1427 (P-Ar aromatic ring in-plane stretching), 1272,1232,1201 (PO stretching), 847 (interaction between aromatic ring vibration and P-C stretching); elemental analysis calculated for $C_{60}H_{50}N_4O_6P_2$ + (2 × CH_3OH) (%): C, 70.98; H, 5.57; N, 5.34; found: C, 70.03; H, 5.60; N, 5.38.

Experimental data for **4ii** (white powder, 22%). M.p.: T > 230ºC (slow decomposition); ^{1}H-NMR (500 MHz, CD_2Cl_2, 25°C): δ (ppm) = 8.18 (bs, 4H), 8.04 (m, $^3J_{H-P}$ ~ 14 Hz, $^3J_{H-H}$ ~ 7.3 Hz, $^4J_{H-H}$ ~ 1.2 Hz, 4H), 7.71 (m, $^3J_{H-H}$ ~ 7.3 Hz, $^4J_{H-H} \approx {}^5J_{H-P}$ ~ 1.2 Hz, 2H), 7.61 (m, $^3J_{H-H}$ ~ 7.3 Hz, $^4J_{H-P}$ ~ 4.8 Hz, 4H), 7.24 (t, $^3J_{H-H}$ ~ 7.9 Hz, 4H), 7.02 (d, $^3J_{H-H}$ ~ 7.9 Hz, 4H), 6.96 (d, $^3J_{H-H}$ ~ 7.9 Hz, 4H), 6.94 (s, 4H), 6.17 (d, $^4J_{H-H}$ ~ 2.55 Hz, 4H), 6.05 (d, $^4J_{H-H}$ ~ 2.55 Hz, 4H), 1.80 ppm (s, 12H); ^{31}P-NMR (500 MHz, CD_2Cl_2, 25°C) δ (ppm): 14.64 (s, P(O)); HR-MALDI-MS: *m/z* calculated for $C_{60}H_{50}N_4O_6P_2$ 984.32, found: 984.32; FT-IR ν (cm^{-1}) 3000 (P-CH_{Ar} streaching), 1580 (P-Ar aromatic ring in-plane stretching), 1480-1427 (P-Ar aromatic ring in-plane stretching), 1265,1228,1202 (PO stretching), 942 (interaction between aromatic ring vibration and P-C stretching); elemental analysis calculated for $C_{60}H_{50}N_4O_6P_2$ + (2 × CH_3CN) (%): C, 72.04; H, 5.29; N, 7.88; found: C, 71.44; H, 5.27; N, 7.93.

2.3. Bis-methylene cavitand **5**.

Calix[4]pyrrole **1a** (0.300g, 0.405mmol) and oven-dried K_2CO_3 (0.213g, 1.539mmol) were dissolved in dry DMSO (10 mL). CH_2Br_2 (57µL, 0.806mmol) was added, under nitrogen, and the mixture was stirred at 80ºC for 3 hrs. The solvent was removed *in vacuo* and the crude was washed with water (5 mL) and extracted with CH_2Cl_2 (3 × 5 mL). The residue was purified by semipreparative HPLC (Sunfire prepC 100 x 4.6mm, 5micron), using a 60:40 THF:H_2O mixture as eluant (Retention time=7.9 minutes). From the collected fraction containing the desired compound, THF was evaporated under reduced pressure and the water fraction was lyophilised yielding **5** as a yellowish solid in 10% yield. M.p.: decomposition at T > 160ºC. ^{1}H-NMR (400 MHz, CD_2Cl_2) δ (ppm) 7.67 (bs, 2H), 7.52 (bs, 2H), 7.18 (t, ^{3}J~7.55 Hz, 4H), 6.89 (d, ^{3}J~7.55 Hz, 4H), 6.81 (d, ^{3}J~7.55 Hz, 4H), 6.60 (bs, 4H), 6.14 (d, ^{4}J~2.60 Hz, 4H), 5.88 (bs, 4H+2H), 5.55 (d, J_{gem}~7.18 Hz, 2H), 1.96 (s, 12H). ^{13}C-NMR (500 MHz, CD_2Cl_2) δ (ppm) 28.32, 44.6, 92, 105.75, 117.07, 118.27, 121.21, 128.71, 137.2, 138.1, 150.7, 156.1; ESI-TOF ES+: m/z calculated for $C_{50}H_{44}N_4O_4$ ($[M+H]^+$) 765.34, found 765.3 $[M+H]^+$.

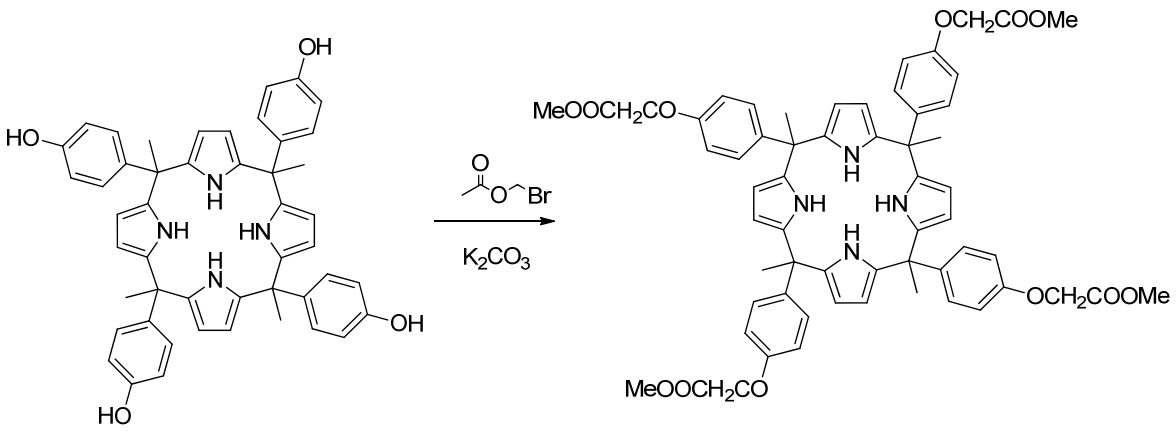

Scheme S3. Synthetic scheme for the preparation of **6**.

2.4. Aryl-extended calix[4]pyrrole **6**[3].

para-Hydroxyphenylmethylcalix[4]pyrrole (1.0g, 1.35mmol) and dry K_2CO_3 (1.2g, 8.68mmol) were suspended in dry acetone (90 mL) and stirred for two hours. Methyl bromoacetate (1.3g, 8.7mmol) was added and the suspension was refluxed for 5 days. After cooling, the solution was filtered off to remove K_2CO_3, and the solvent removed *in vacuo*. The orange product obtained was dissolved in dichloromethane (100 mL) and washed with water (100 mL). The organic phase was dried over $MgSO_4$ and the solvent removed *in vacuo* affording an oil which was triturated with ethanol. The product was obtained as a white powder by filtration and dried under high vacuum (70% yield). ^{1}H-NMR (400.1 MHz, CD_2Cl_2) δ (ppm) 7.7 (bs, 4H), 7.07 (d, 8H), 6.80 (d, 8H), 5.77 (d, 8H), 4.65 (s, 8H), 3.81 (s, 12H), 1.55 (s, 12H). ^{13}C-NMR 400.1 MHz δ (ppm) CD_2Cl_2: 18.1, 27.6, 44.1, 52.0, 65.2, 106.2, 113.5, 128.6, 136.6, 141.3, 156.3, 169.2.

3. NMR spectra of *bis*-phosphonate calix[4]pyrroles 4.

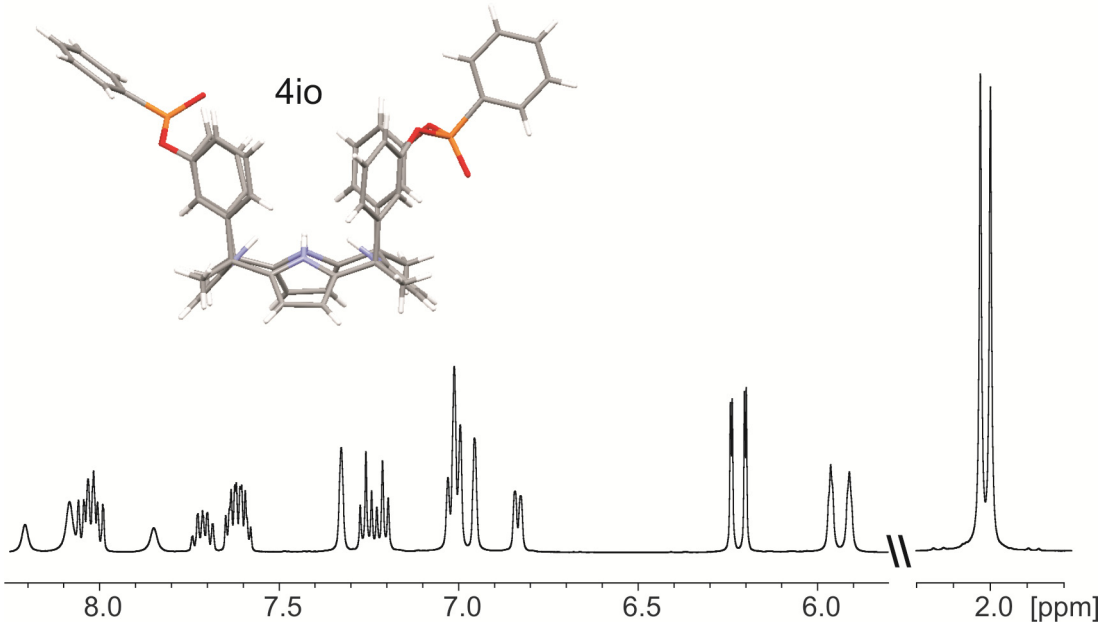

Figure S2. ^{1}H-NMR spectrum of the **4io** stereoisomer in dichloromethane-d_2 solution at 298 K.

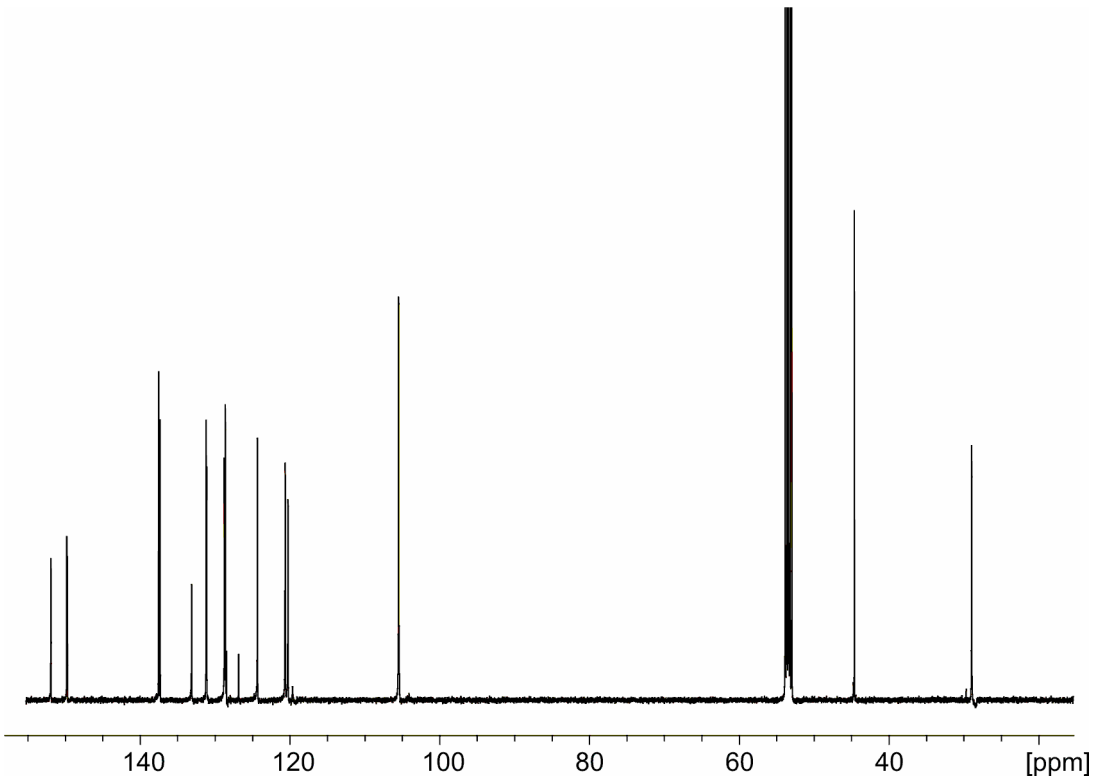

Figure S3. ^{13}C-NMR spectrum of the **4io** stereoisomer in dichloromethane-d_2 solution at 298 K.

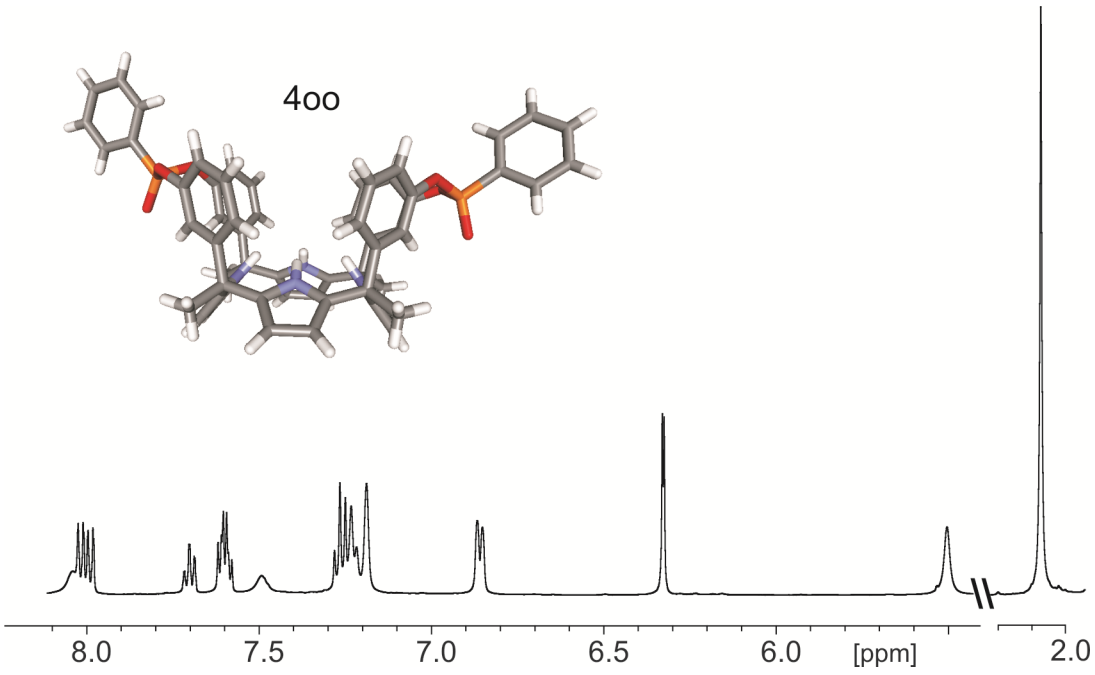

Figure S4. [1]H-NMR spectrum of the **4oo** stereoisomer in dichloromethane-d_2 solution at 298 K.

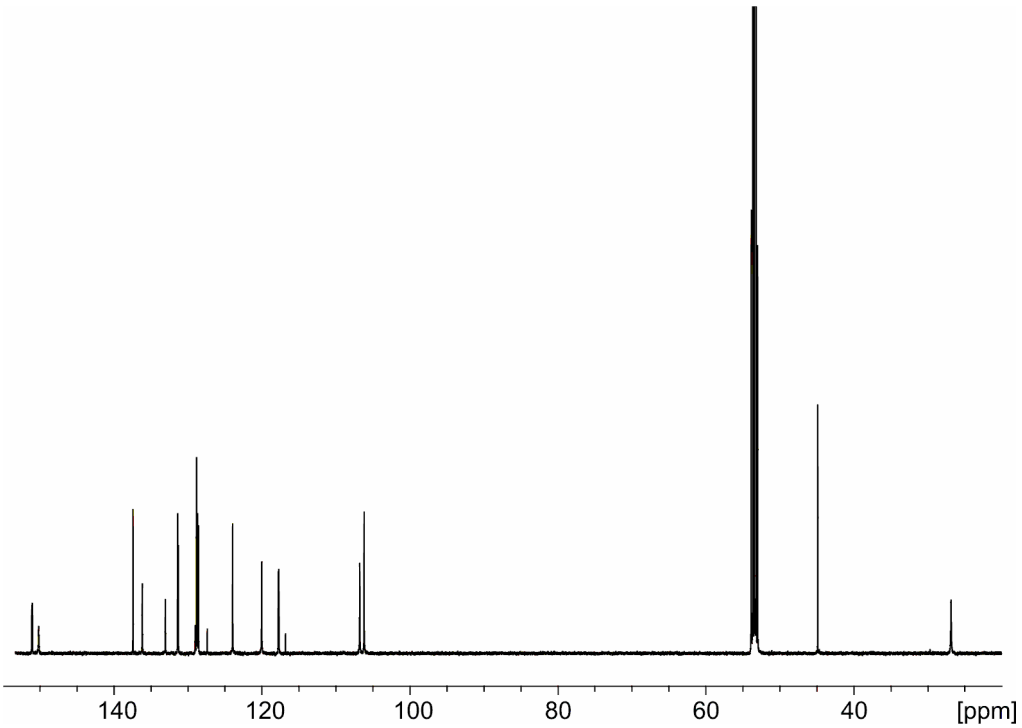

Figure S5. [13]C-NMR spectrum of the **4oo** stereoisomer in dichloromethane-d_2 solution at 298 K.

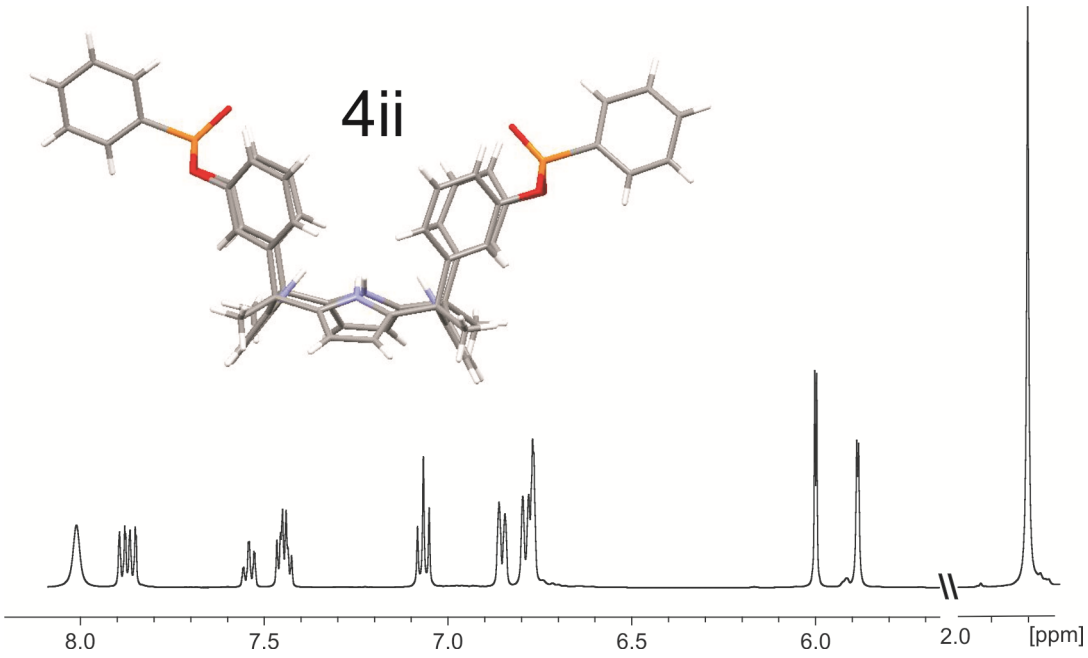

Figure S6. ^{1}H-NMR spectrum of the **4ii** stereoisomer in dichloromethane-*d* solution at 298 K.

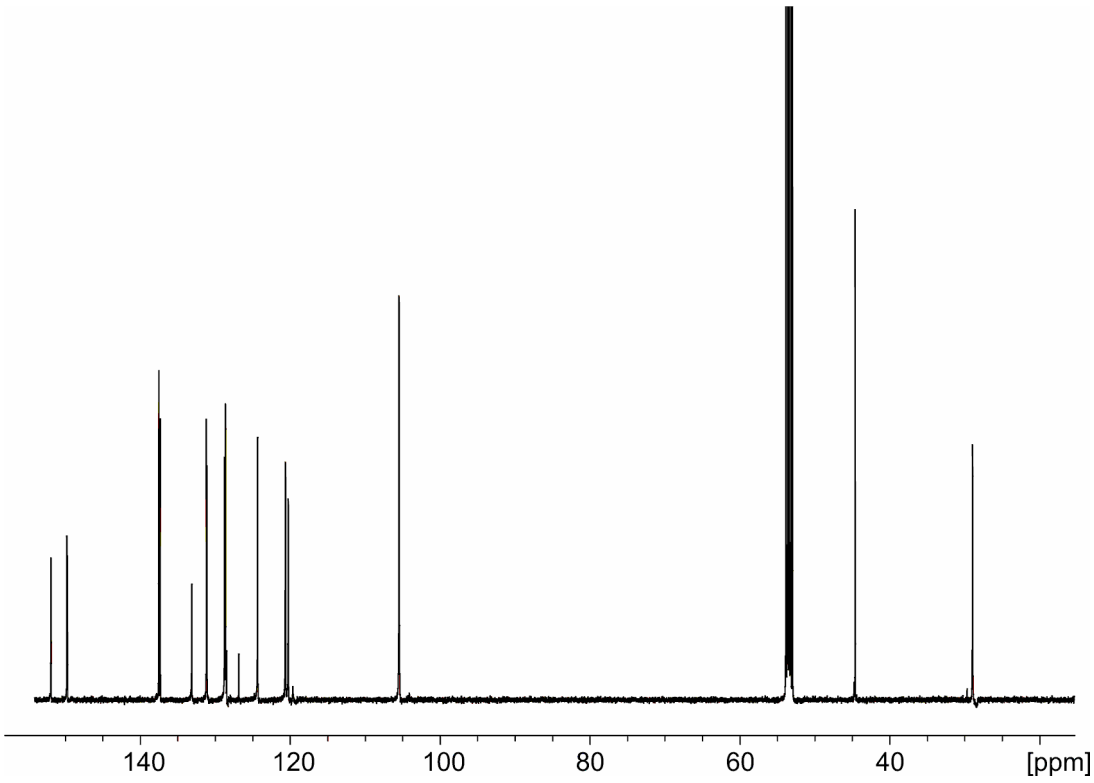

Figure S7. ^{13}C-NMR spectrum of **4ii** stereoisomer in dichloromethane-d_2 solution at 298 K.

4. Data fitting for the dilution experiments of *bis*-phosphonate calix[4]pyrroles 4 in DCM solution.

Receptors **4** showed a moderate tendency for aggregation in DCM solution. We performed dilution experiments in the range of 1 mM to 14 mM using ^{1}H NMR spectroscopy. The fit of the chemical shift changes observed for selected signals of the protons to a simple dimerization model allowed us to estimate dimerization constant values of the order 10-50 M^{-1}. We considered the tendency to aggregation (< 10%) observed for these receptors to be negligible at the concentrations (~ 1mM) typically used for the binding experiments (Figures S8-S10).

^{1}H NMR dilution experiments of *bis*-phosphonate calix[4]pyrroles in DCM solution.

The ^{1}H NMR dilution experiments of **4** were carried out on a Bruker 400MHz spectrometer, at 298 K. Solutions were prepared by weighting separately the three diastereoisomers in three different volumetric flasks of 1 mL in order to make a moderately concentrated stock solution (**4ii**: 13.2 mM; **4oo**: 17.6 mM; **4io**: 14.2 mM). A ^{1}H NMR spectrum of 0.5 mL of **4ii**, **4oo** and **4io** stock solution was recorded for each stereoisomer. Then each NMR tube solution was sequentially diluted by transferring specific volumes of solvent by a volumetric pipette, for a total of three sequential dilutions per host solution (8 mM; 5 mM; 1 mM). The oligomerization process shows a fast exchange in the NMR timescale in all cases, and the constants were determined by monitoring the chemical shift changes of the β- pyrrolic protons as incremental volume of solvent was added. The value of the association constant was calculated using the software HyperNMR.

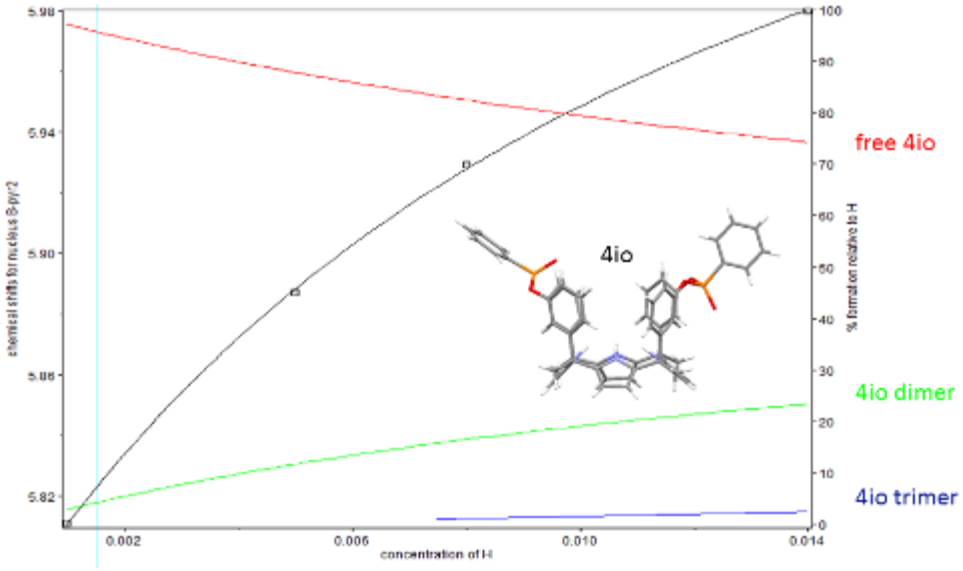

Figure S8. Plot of the chemical shift changes experienced by the signal of one of the aromatic protons in the *meso*-phenyl substituent of **4io** (black squares) upon dilution. Fit (solid black curve) of the experimental data to a theoretical oligomerization model including three species: monomer, dimer and trimer. The speciation curves corresponding to the dilution experiment are also shown with different colors for each species: monomer (red), dimer (green) and trimer (blue). The highest concentration of **4io** used in the titrations experiments was 5 mM. At this concentration the amount of trimer is negligible and less than 15 % of **4io** is involved in the formation of the dimer.

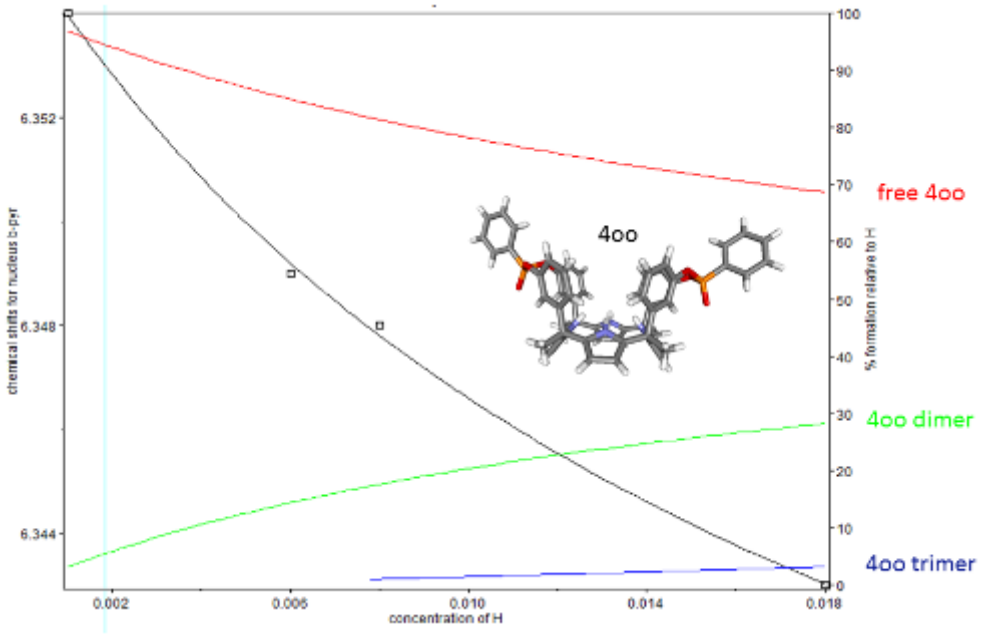

Figure S9. Plot of the chemical shift changes experienced by the signal of one of the aromatic protons in the *meso*-phenyl substituent of **4io** (black squares) upon dilution. Fit (solid black curve) of the experimental data to a theoretical oligomerization model including three species: monomer, dimer and trimer. The speciation curves corresponding to the dilution experiment are also shown with different colors for each species: monomer (red), dimer (green) and trimer (blue). The highest concentration of **4oo** used in the titrations experiments was 5 mM. At this concentration the amount of trimer is negligible and less than15 % of **4oo** is involved in the formation of the dimer.

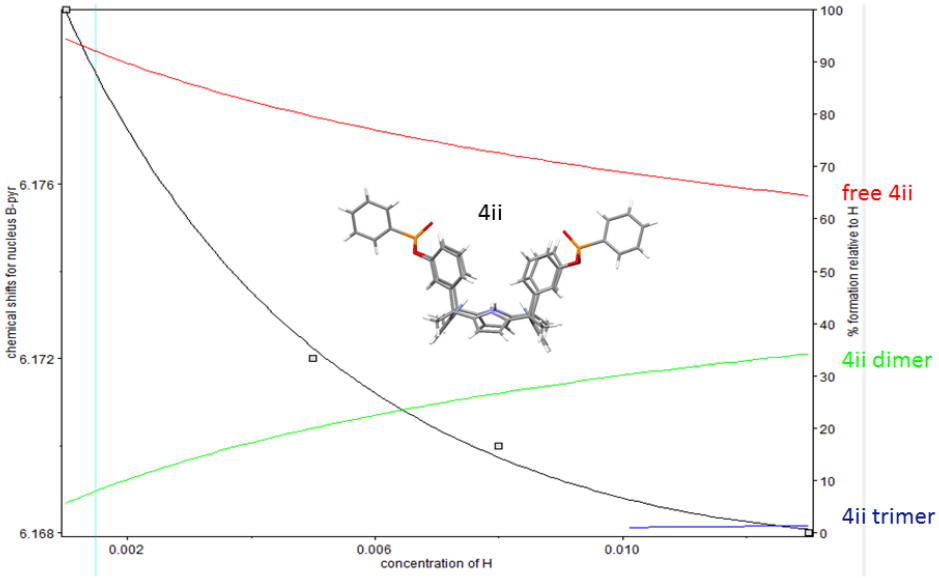

Figure S10. Plot of the chemical shift changes experienced by the signal of one of the aromatic protons in the *meso*-phenyl substituent of **4ii** (black squares) upon dilution. Fit (solid black curve) of the experimental data to a theoretical oligomerization model including three species: monomer, dimer and trimer. The speciation curves corresponding to the dilution experiment are also shown with different colors for each species: monomer (red), dimer (green) and trimer (blue). The highest concentration of **4ii** used in the titrations experiments was 5 mM. At this concentration the amount of trimer is negligible and less than 20 % of **4ii** is involved in the formation of the dimer.

5. NMR spectra of the binding studies of cavitans 4 with different alkylphosphonium/ammonium salts in DCM solution.

5.1. Binding of bis-phosphonate calix[4]pyrroles **4** with TMPCl.

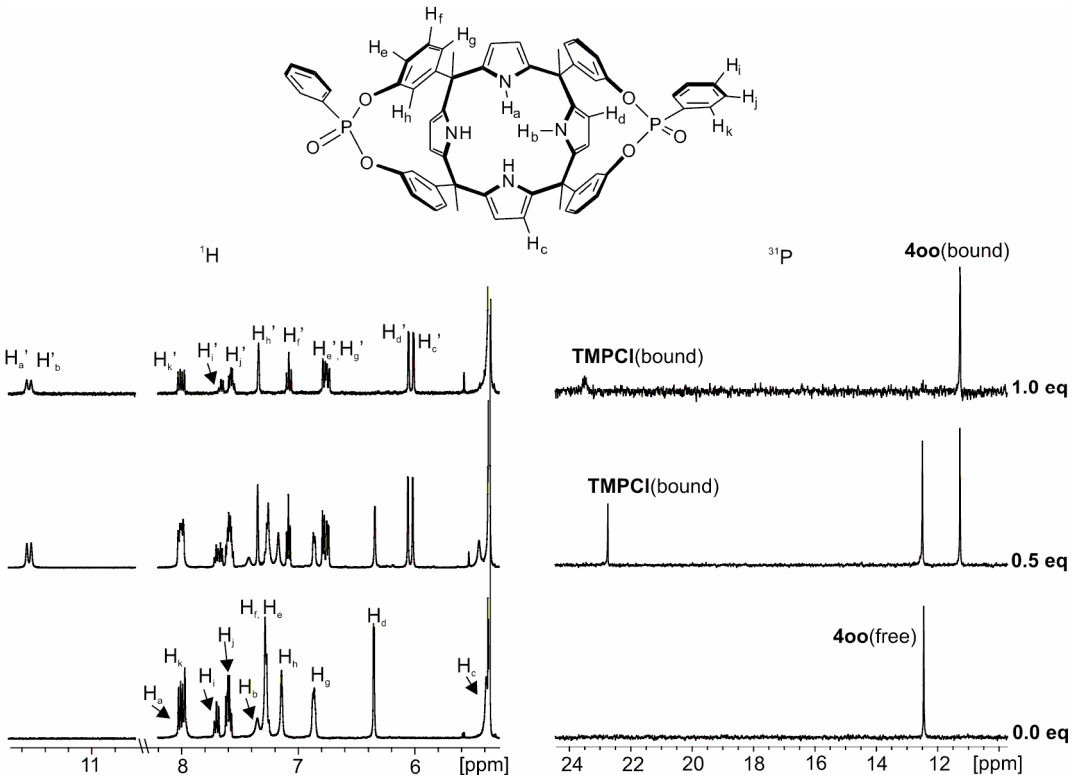

Figure S11. Selected regions of the ^{1}H-NMR and ^{31}P-NMR spectra of a 4.6mM dichloromethane solution of **4oo** after the addition of 0, 0.5 and 1.0 equivalent of TMPCl.

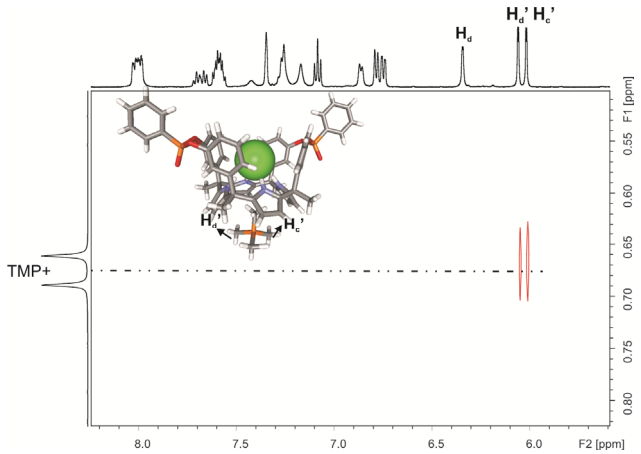

Figure S12. Selected region of the 2D-ROESY experiment performed on a 4.6mM dichloromethane solution of **4oo** with 0.5 equivalents of TMPCl. The observed intermolecular nOe cross-peak between the protons of TMP^{+} and the *β*-pyrrolic protons (Hd', Hc') of bound **4oo** indicate that the cation is preferentially located in the calix[4]pyrrole cup opposite to the bound chloride.

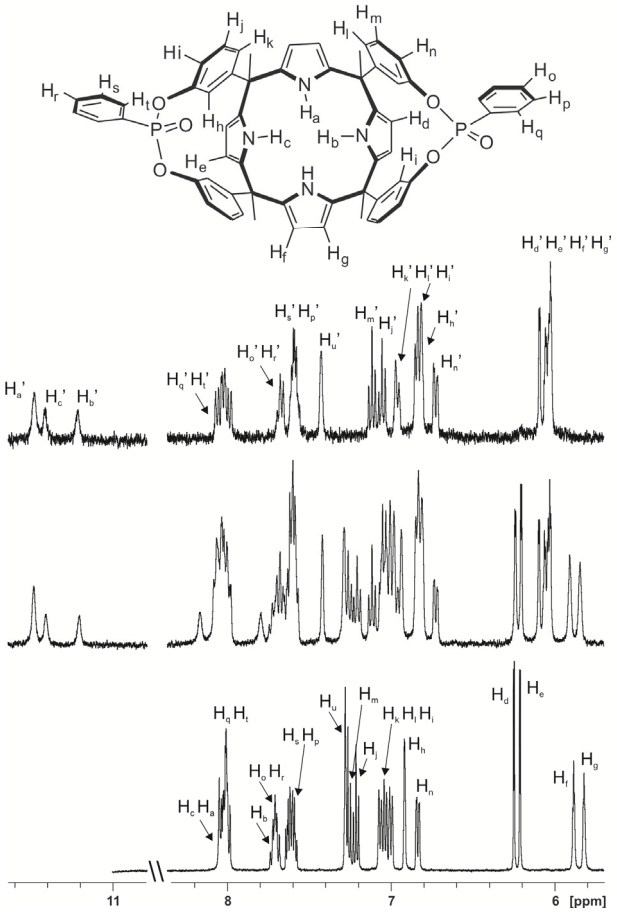

Figure S13. Selected regions of ^{1}H-NMR and ^{31}P-NMR spectra of a 4.6mM dichloromethane solution of **4io** after the addition of 0, 0.5 and 1.0 equivalents of TMPCl.

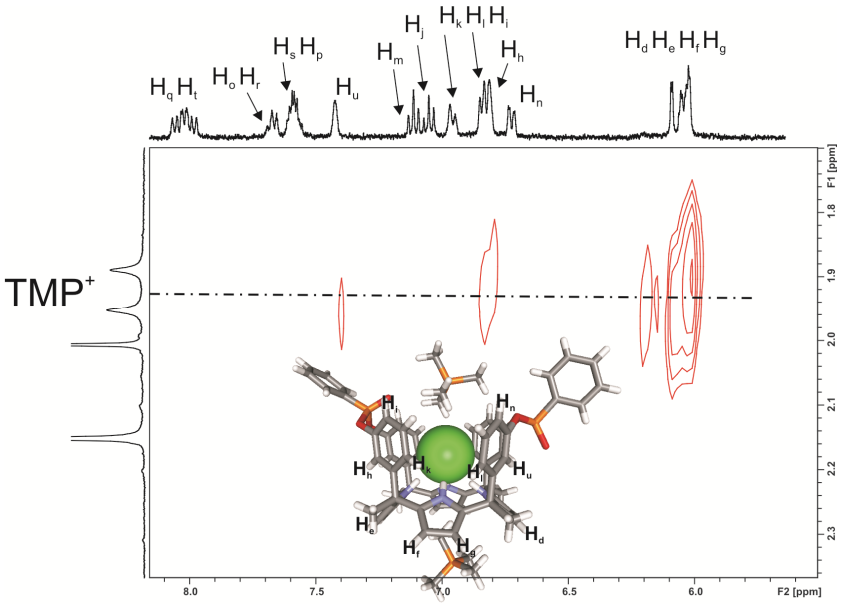

Figure S14. Selected region of a 2D-ROESY experiment performed on a 4.6mM dichloromethane solution of **4io** with 1.0 equivalents of TMPCl. The observed intermolecular nOe cross peaks between the protons of the TMP^{+} and both the *β*-pyrrolic protons and the *meso*-phenyl protons of bound **4io** indicate that placement of the cation within the ion-paired complex can take place in two possible binding sites.

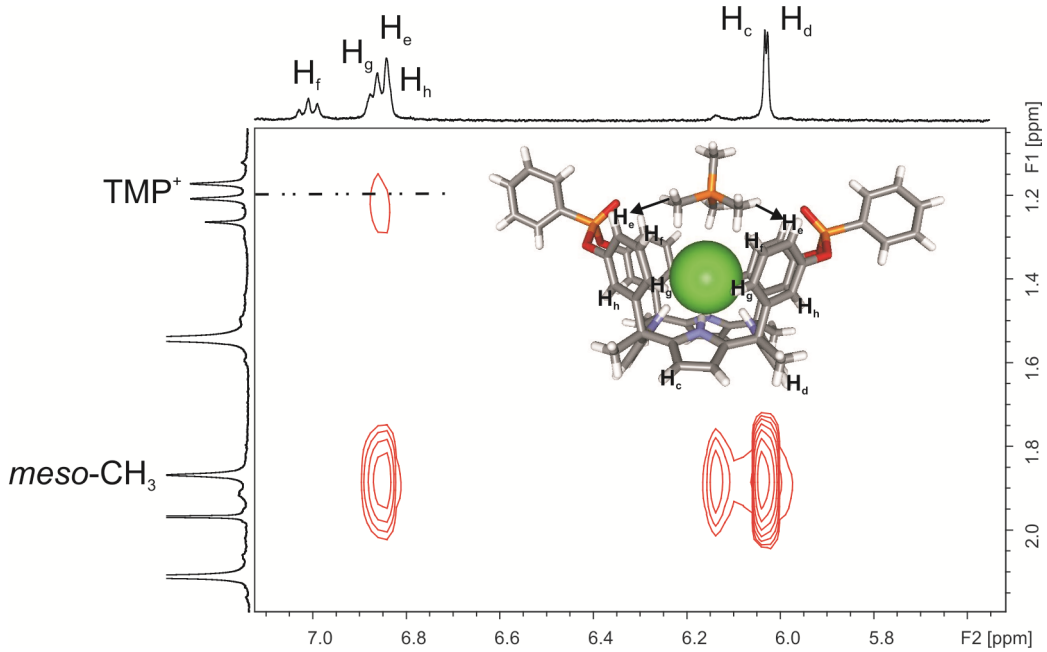

Figure S15. Selected region of a 2D-ROESY experiment performed on a 4.6mM dichloromethane solution of **4ii** containing 0.9 equivalents of TMPCl. The intermolecular nOe cross peaks observed between the signal of the protons of TMP^+ and the *meso*-phenyl protons (He) of **4ii** is indicative of the preferred close-contact arrangement for the ion-pair in the 1.1 complex.

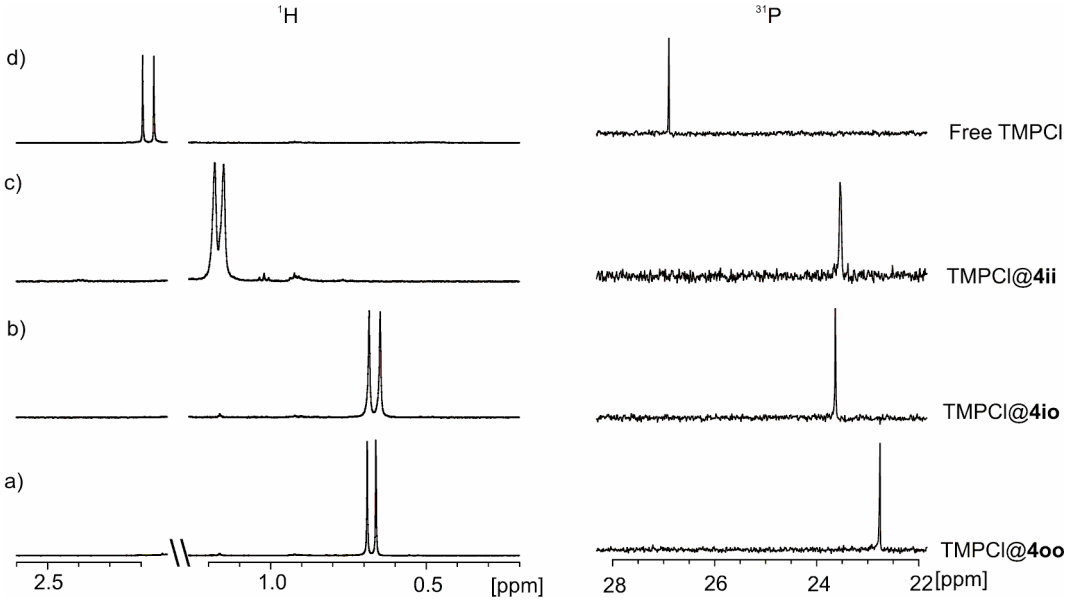

Figure S16. Selected regions of the ^{1}H-NMR and ^{31}P-NMR spectra of a 4.6mM dichloromethane solution of a) **4oo**, b) **4io** and c) **4ii** with 0.5 equivalents of TMPCl added, d) free TMPC.

6. Pairwise competitive binding experiments of bis-phosphonate calix[4]pyrroles 4 and TMPCl.

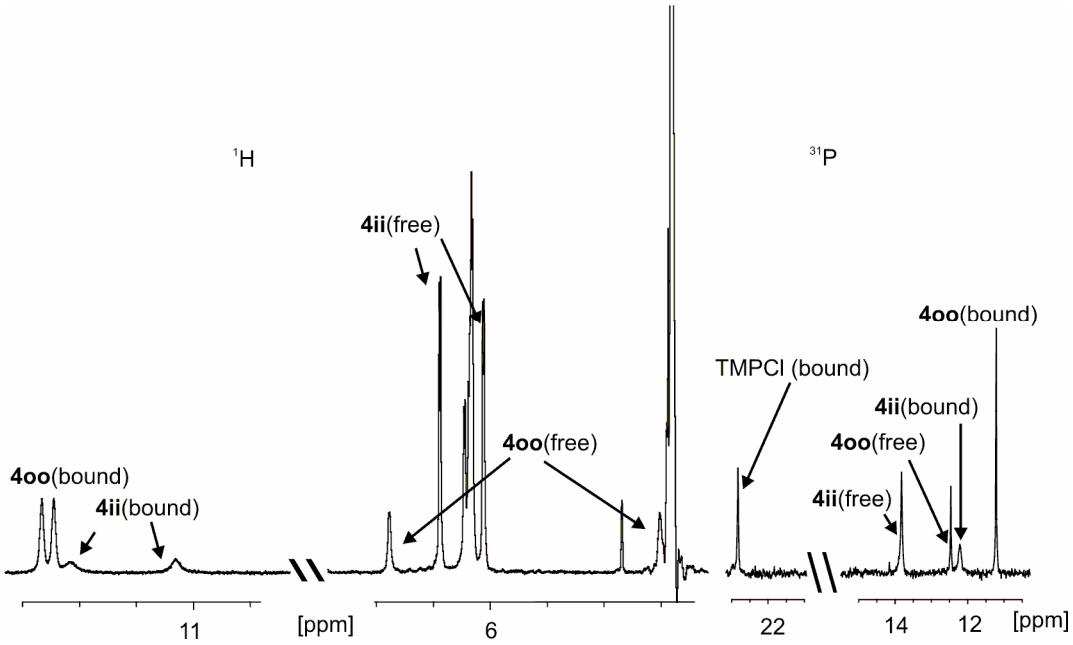

Figure S17. Selected regions of the ^{1}H-NMR and ^{31}P-NMR spectrum of an equimolar mixture of **4oo**, **4ii** and TMPCl in DCM-d_2 solution.

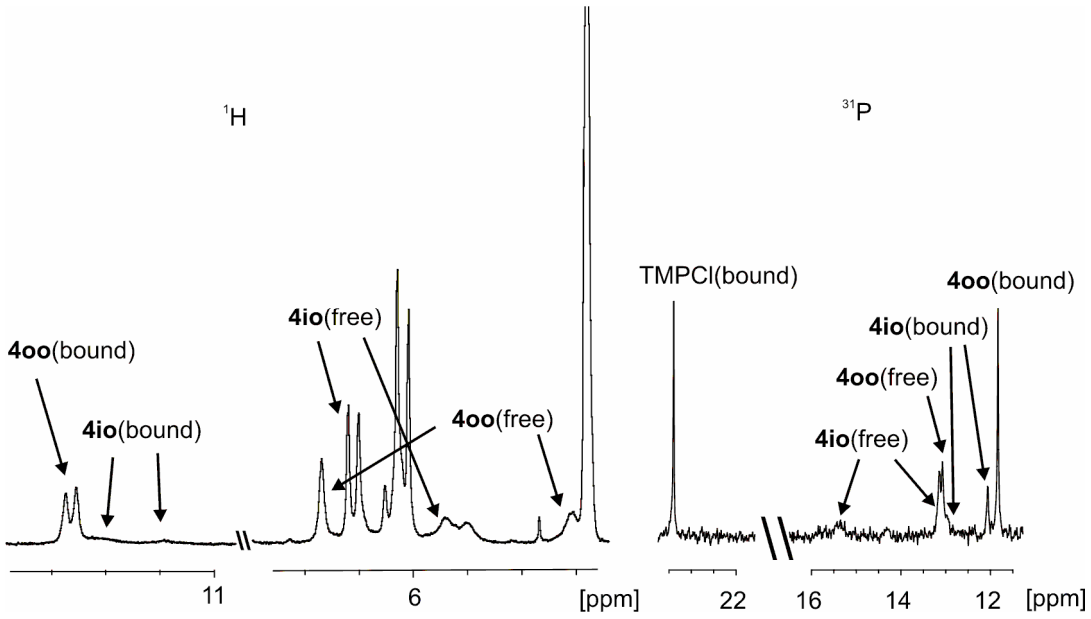

Figure S18. Selected regions of the ^{1}H-NMR and ^{31}P-NMR spectrum of an equimolar mixture of **4oo**, **4io** and TMPCl in DCM-d_2 solution.

7. Pairwise competitive binding experiments of bis-phosphonate calix[4]pyrroles 4, bis-methylene calix[4]pyrrole 5 and aryl-extended calix[4]pyrrole 6 with TMPCl.

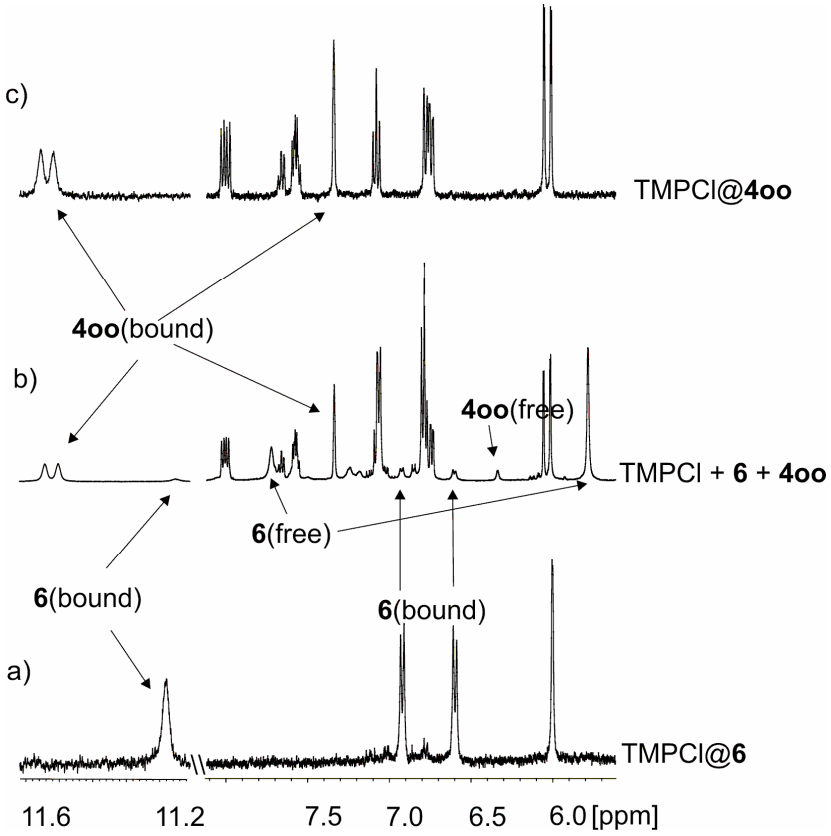

Figure S19. Selected regions of the ^{1}H-NMR spectra in DCM-d_2 solution of: a) TMPCl@**6**, b) an equimolar mixture of TMPCl + **6** + **4oo** and c) TMPCl@**4oo**.

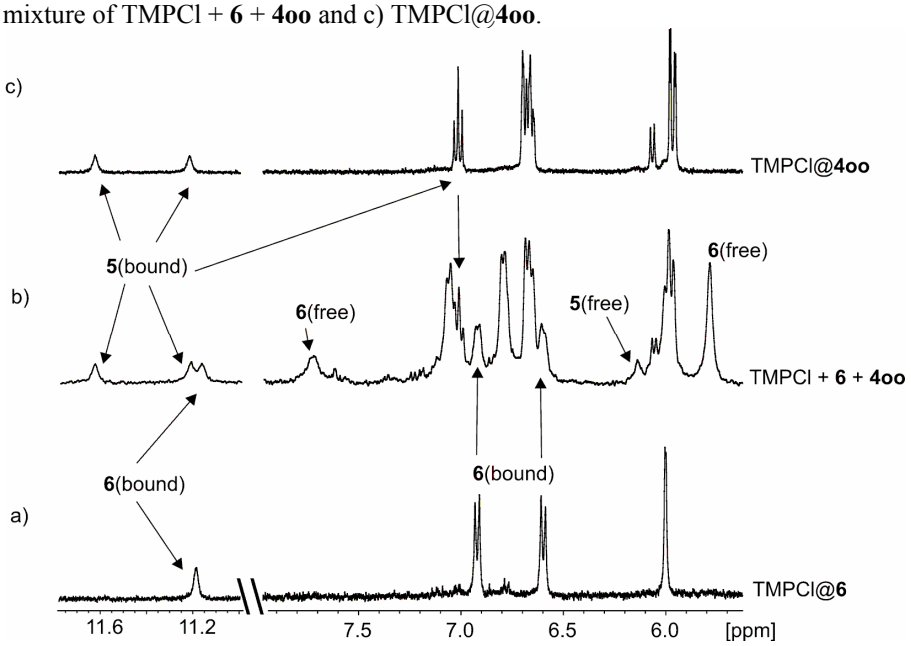

Figure S20. Selected regions of the ^{1}H-NMR spectra in DCM-d_2 solution of: a) TMPCl@**6**, b) an equimolar mixture of TMPCl + **6** + **5** and c) TMPCl@**5**.

7.1. Pairwise competitive binding experiments of bis-phosphonate calix[4]pyrroles 4 and DTMACl.

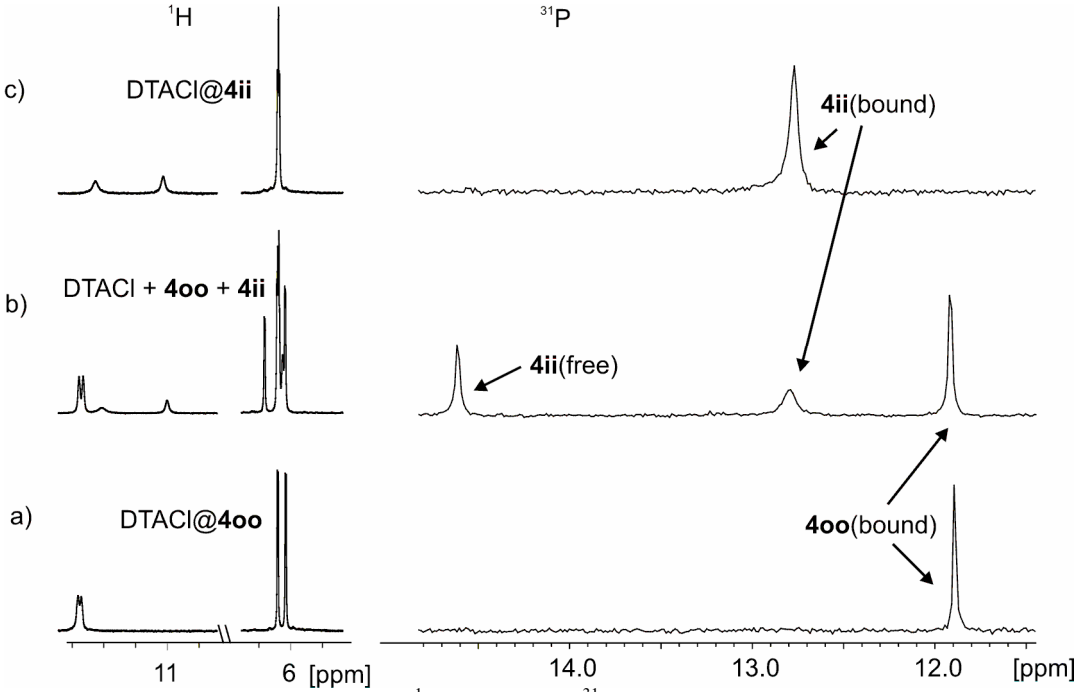

Figure S21. Selected regions of the ^{1}H-NMR and ^{31}P-NMR spectra in DCM-d_2 solutions of a) DTACl@**4oo**, b) an equimolar mixture of DTACl + **4oo** + **4ii**, c) DTACl@**4ii**.

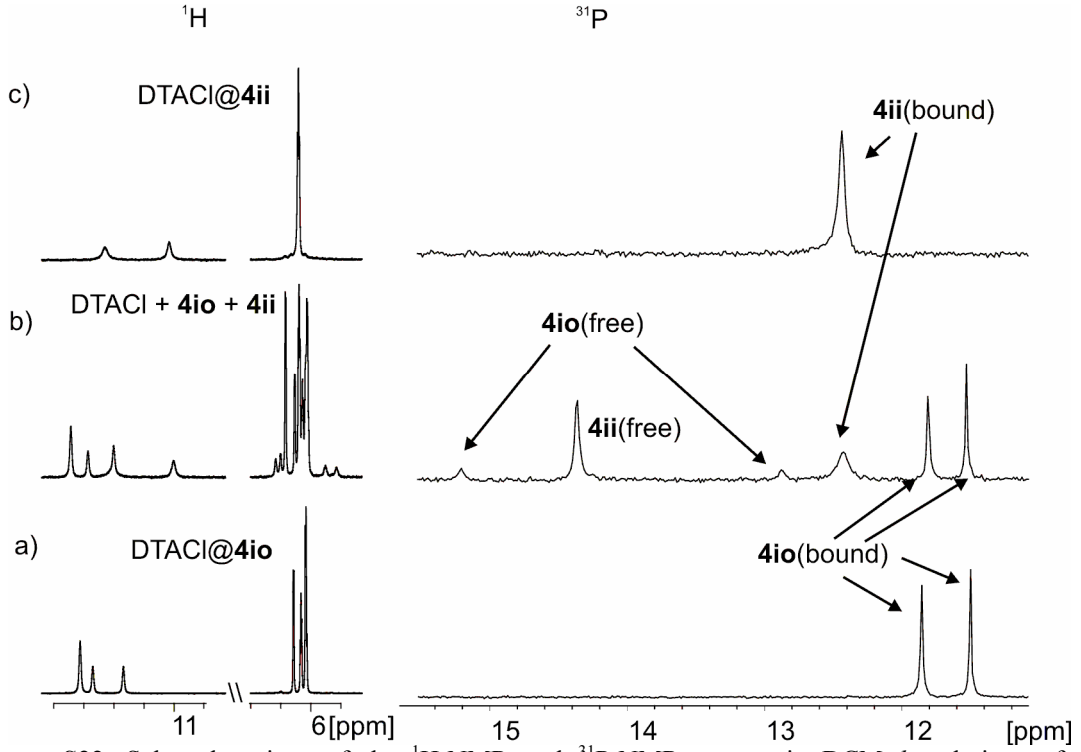

Figure S22. Selected regions of the ^{1}H-NMR and ^{31}P-NMR spectra in DCM-d_2 solutions of: a) DTACl@**4io**, b) an equimolar mixture of DTACl + **4io** + **4ii**, c) DTACl@**4ii**.

7.2. Bis-phosphonate calix[4]pyrroles 4 binding TBACl.

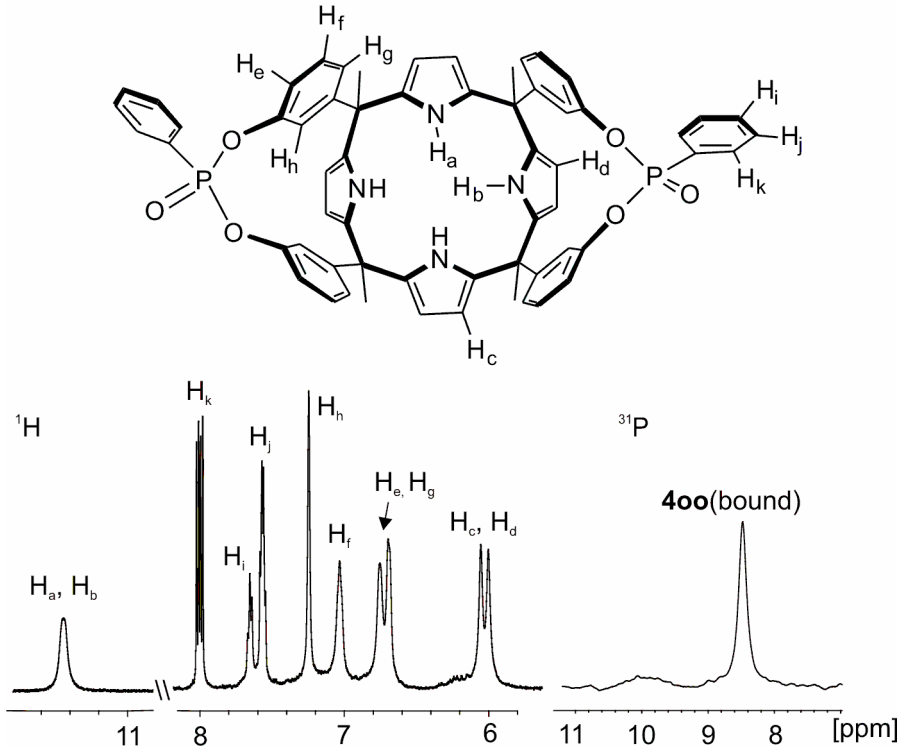

Figure S23. Selected regions of the ^{1}H-NMR and ^{31}P-NMR spectra of a 3.45mM solution of **4oo** in DCM- d_2 solution after addition of 0.95 equivalents of TBACl.

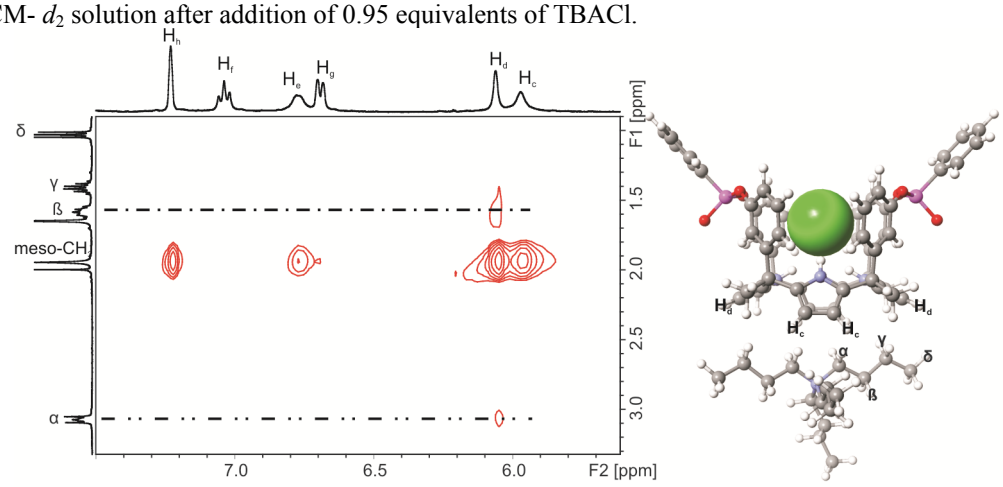

Figure S24. Selected region of the 2D-ROESY experiment performed on a 4.12mM DCM-d_2 solution of **4oo** with 1.0 equivalents of TBACl. The observed nOes between the α and β protons of TBA^{+} with the *β*-pyrrolic protons (Hd) of bound **4oo** indicate that the cation is located in the cup of the calix[4]pyrrole opposite to the bound anion. The CAChe energy minimized structure of TBACl@**4oo** is shown at the right.

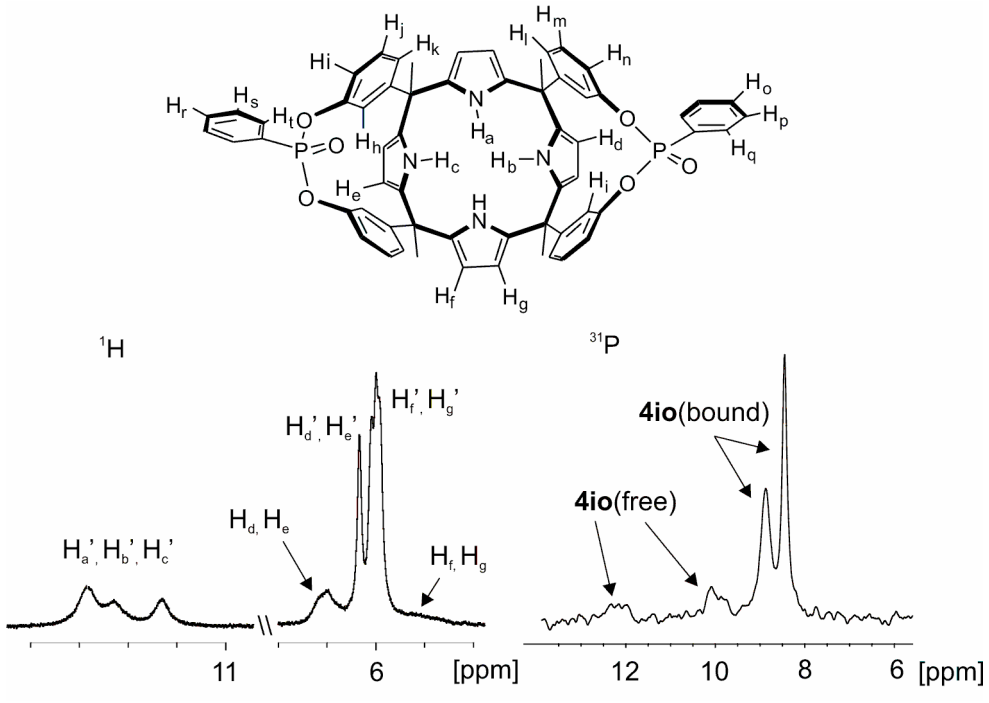

Figure S25. Selected regions of the ^{1}H-NMR and ^{31}P-NMR spectra of a 3.45mM solution of **4io** in DCM-d_2 solution after addition of 0.95 equivalents of TBACl.

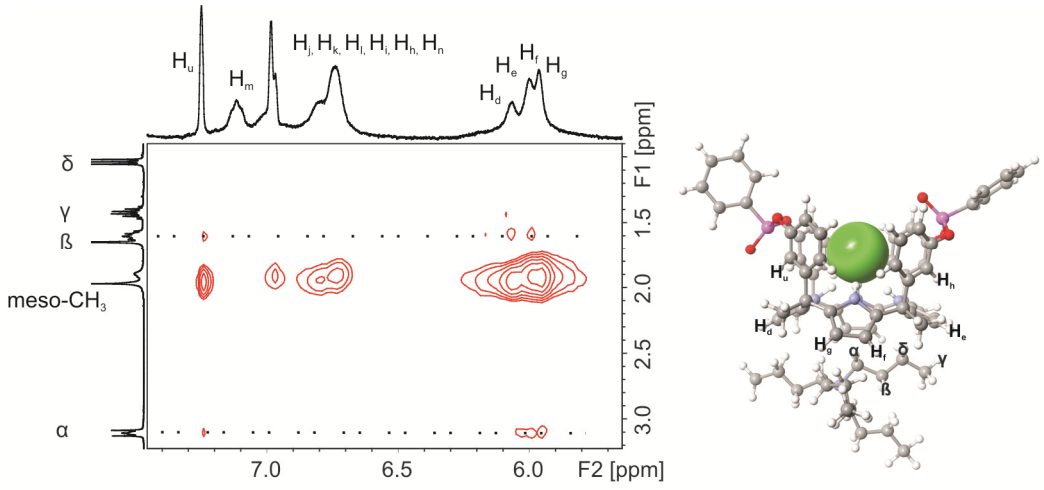

Figure S26. Selected region of the 2D-ROESY experiment performed on a 4.12mM DCM-d_2 solution of **4io** with 1.0 equivalents of TBACl. The observed nOes between the α and β protons of TBA^{+} with the *β*-pyrrolic protons (Hd) of bound **4io** indicate that the cation is located in the cup of the calix[4]pyrrole opposite to the bound anion. The CAChe energy minimized structure of TBACl@**4io** is shown at the right.

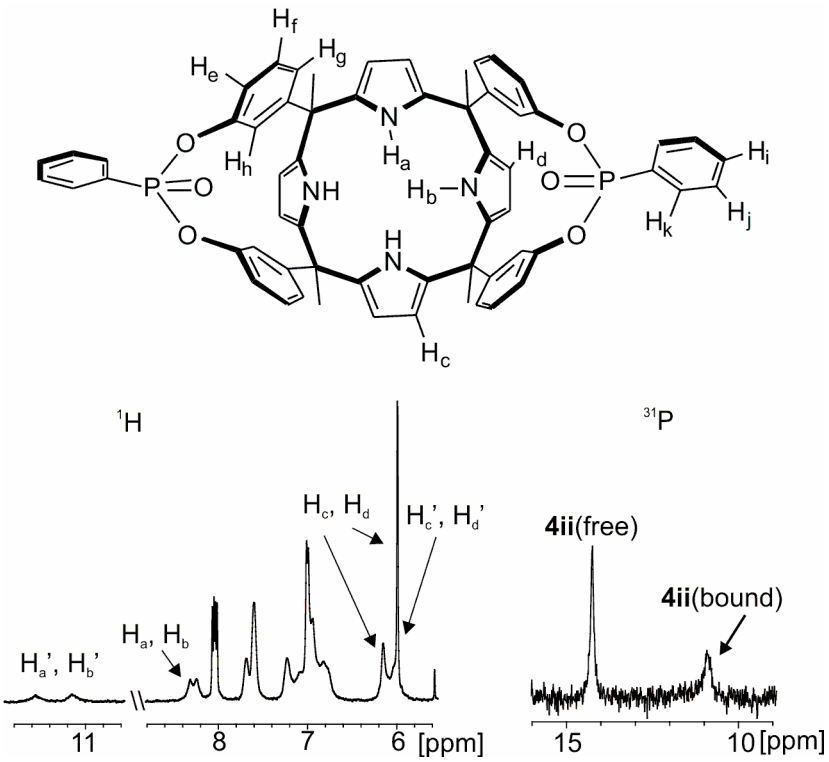

Figure S27. Selected regions of the ^{1}H-NMR ^{31}P-NMR spectraof a 3.0mM DCM-d_2 solution of **4ii** after addition of 1.0 equivalents of TBACl in dichloromethane.

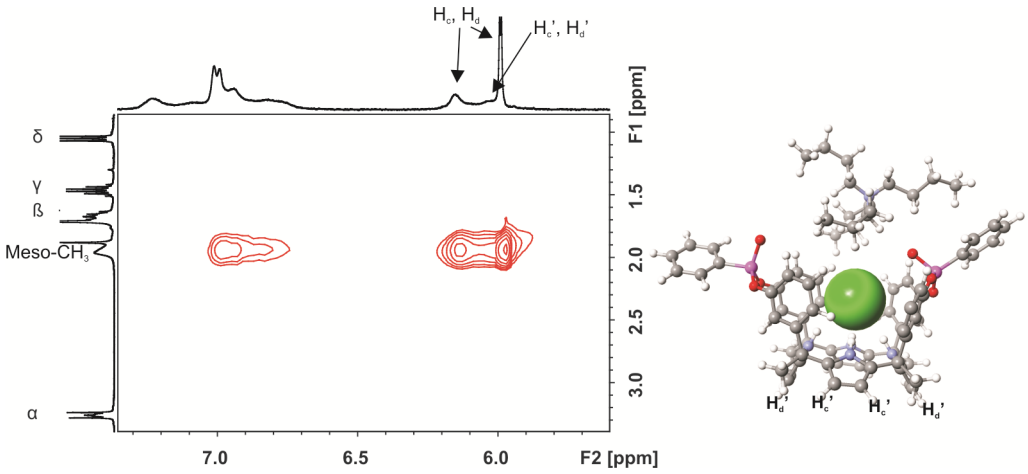

Figure S28. Selected region of a 2D-ROESY experiment performed on a 3.614mM dichloromethane-d_2 solution of **4ii** with 1.2 equivalents of TBACl. No nOe cross peaks were observed between the protons of TBA^{+} and the signals of **4ii**.

7.3. Pairwise competitite binding experiments of bis-phosphonate calix[4]pyrroles 4 with OAMCl.

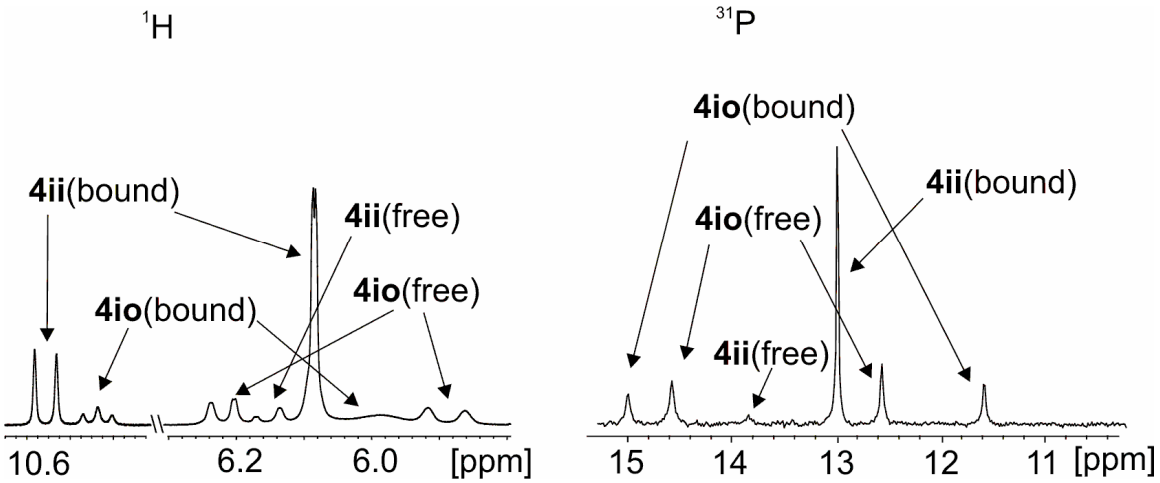

Figure S29. Selected regions of ^{1}H-NMR and ^{31}P-NMR spectra of an equimolar mixture of **4ii**, **4io** and octylammonium chloride in DCM-d_2 solution.

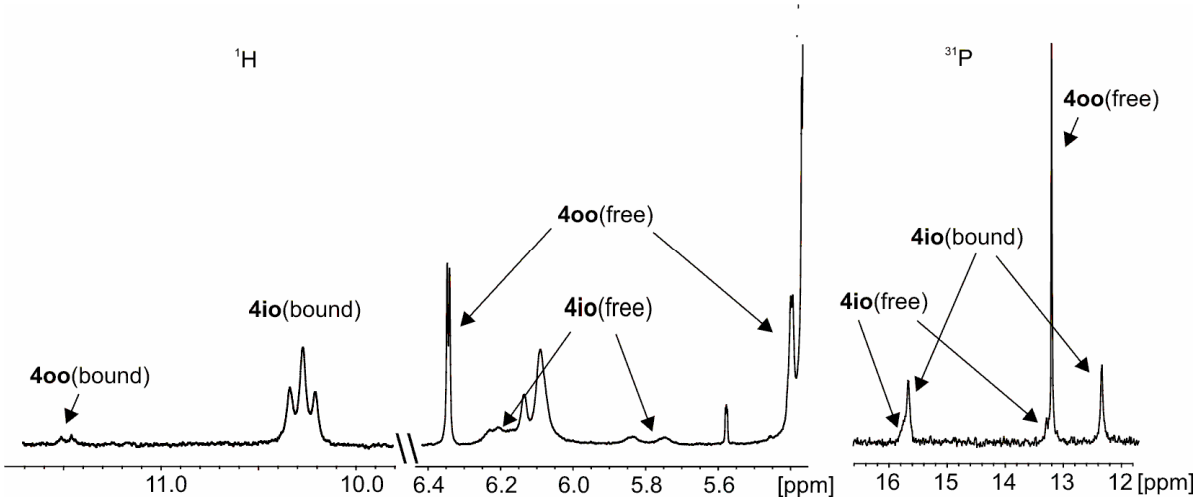

Figure S30. Selected regions of ^{1}H-NMR and ^{31}P-NMR spectra of an equimolar mixture of **4io**, **4oo** and octylammonium chloride in DCM-d_2 solution.

8. Fit of the ^{1}H NMR titration data of 6 with TBACl to a 1:1 binding model.

^{1}H NMR binding experiment of **6** with TBACl in DCM solution. The complexation behaviour of **6** toward TBACl was studied by ^{1}H NMR on a Bruker 400MHz spectrometer, at 298 K. The association constant was determined by adding aliquots of a 1.5 x 10^{-1} M solution of TBACl in CD_2Cl_2 into the NMR tube containing a 1.46 x 10^{-2} M solution of **6** in the same solvent. The concentration of the receptor was variable throughout the titration. The complexation of TBACl shows a fast exchange in the NMR timescale. The association constant between **6** and the chloride anion was determined as $K_{a,exp}$ = 1±0.2 × 10^1 M^{-1} by monitoring the chemical changes of the protons resonating at 6.80 ppm (*meso*-phenyl protons) and 4.65 ppm (methylene protons of the lateral chain) in the ^{1}H NMR spectrum as incremental amounts of the guest were added (0.5; 1; 2; 5; 10 equivalents of TBACl). The value of the association constant was calculated using the software HyperNMR. The data were fitted to a simple 1:1 binding model.

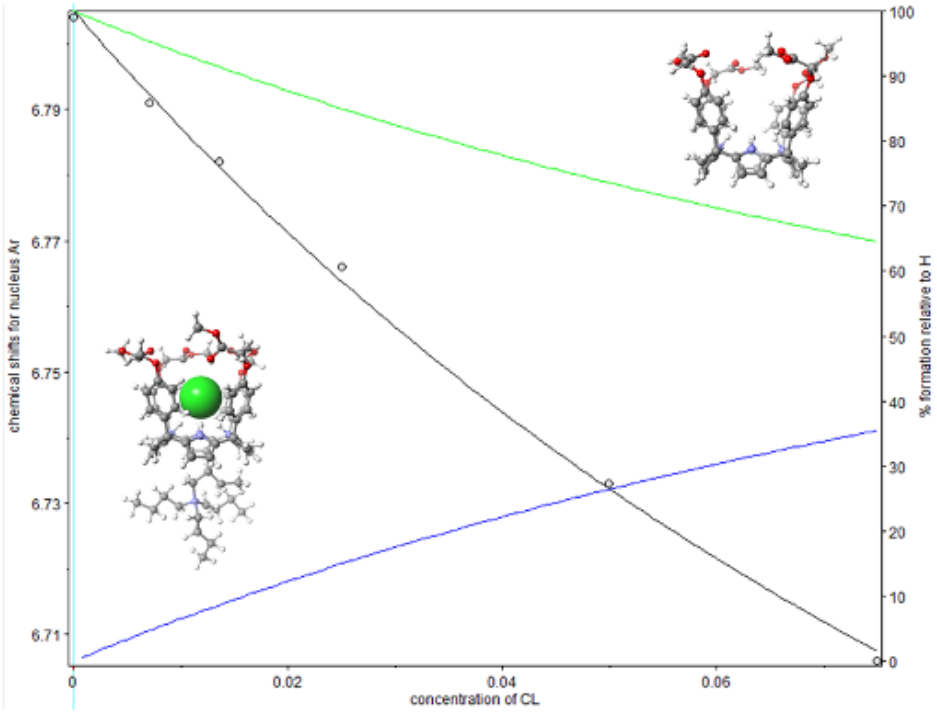

Figure S31. Plot of the chemical shift changes experienced by the signal of the aromatic proton H_c at 6.8 ppm in the *meso*-phenyl substituent of [**6**] = 14.6 mM (black circles) upon titration with incremental amounts of TBACl. Fit (solid black curve) of the experimental data to a theoretical 1:1 binding model. The speciation curves corresponding to the titration experiment are also shown with different colours for each species: free 6 (green), complex (blue).

9. NMR spectra of the binding studies of cavitands 4 and aryl-extended calix[4]pyrrole 6 with TMPCl in ACN solution.

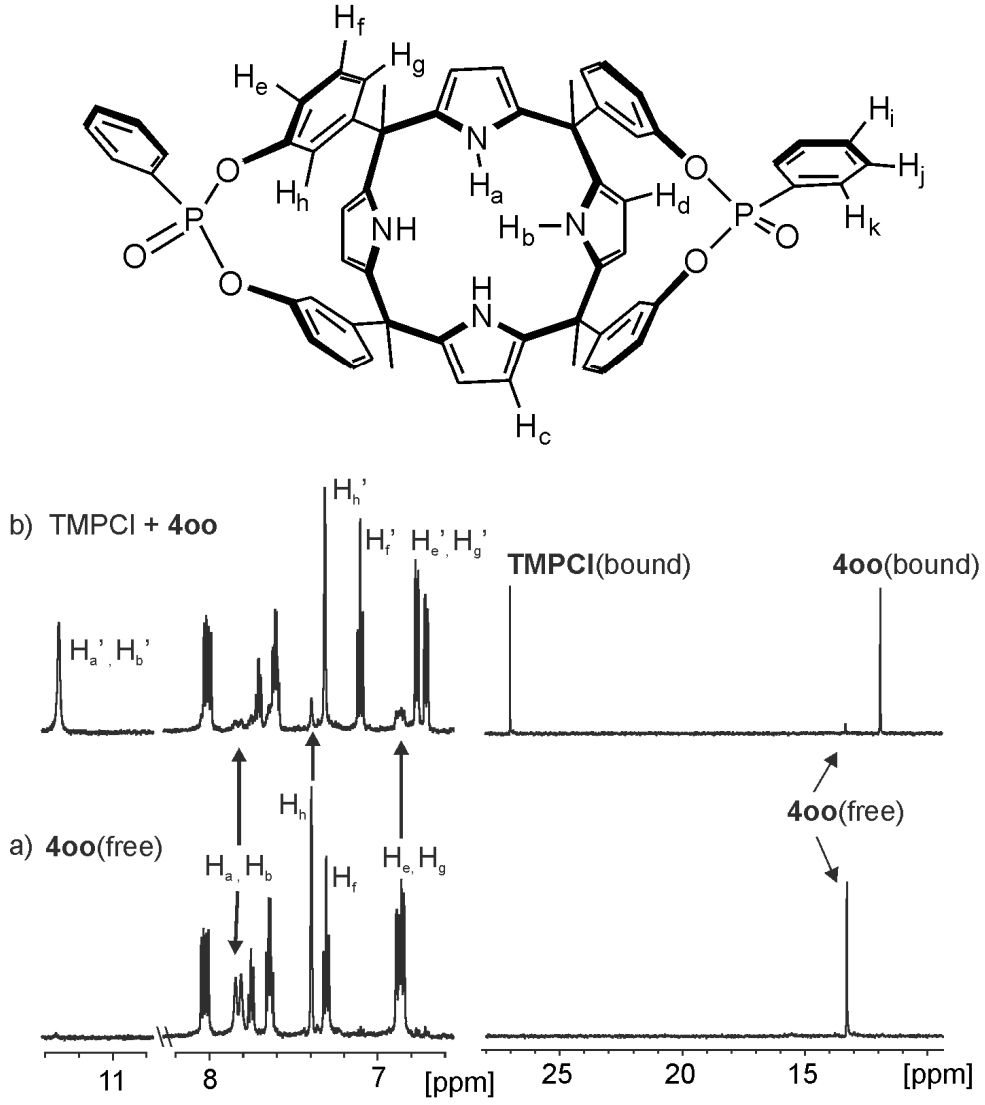

Figure S32. Selected regions of ^{1}H-NMR and ^{31}P-NMR spectra of a 3.03mM solution of **4oo** in ACN-d_3 after addition of a) 0 equivalents and b) 1.0 equivalent of TMPCl.

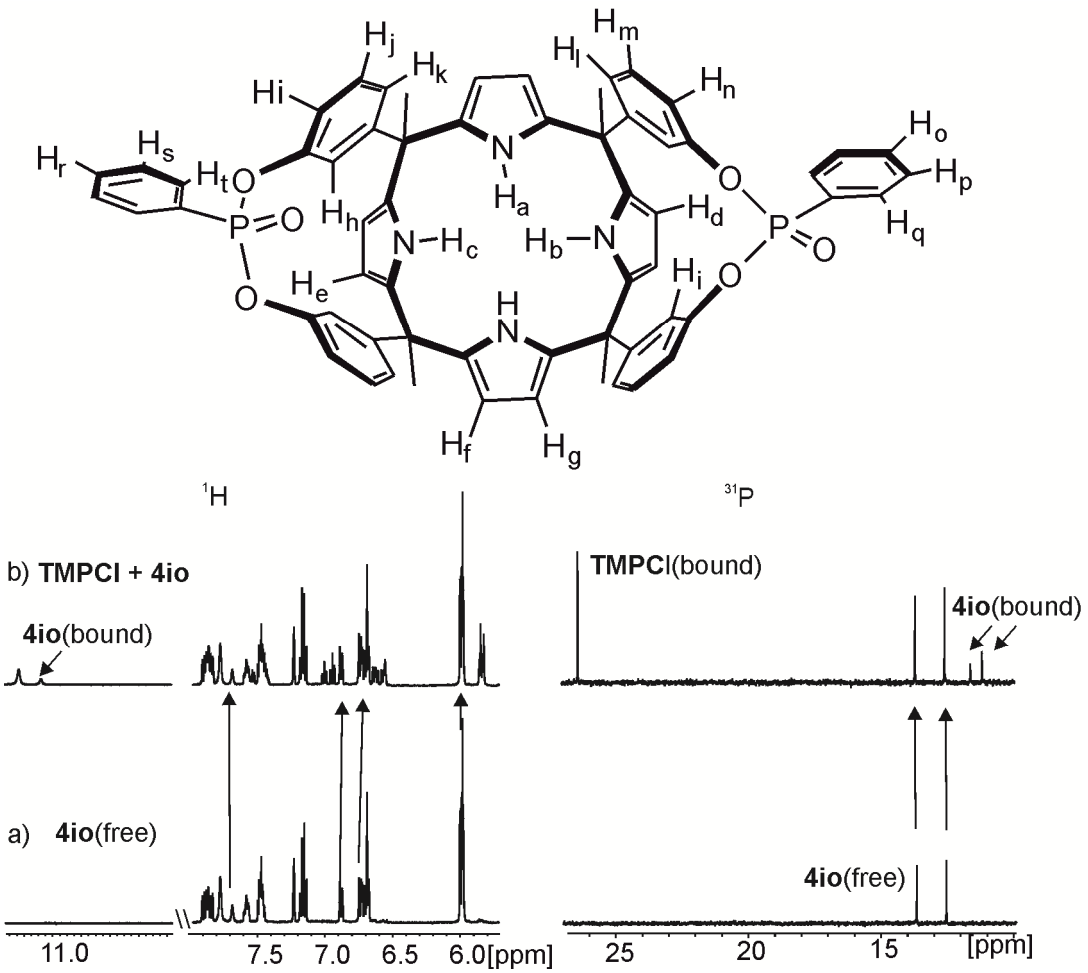

Figure S33. Selected regions of ^{1}H-NMR and ^{31}P-NMR spectra of a 0.327mM solution of **4io** in ACN-d_3 after addition of a) 0 equivalents and b) 1.0 equivalent of TMPCl.

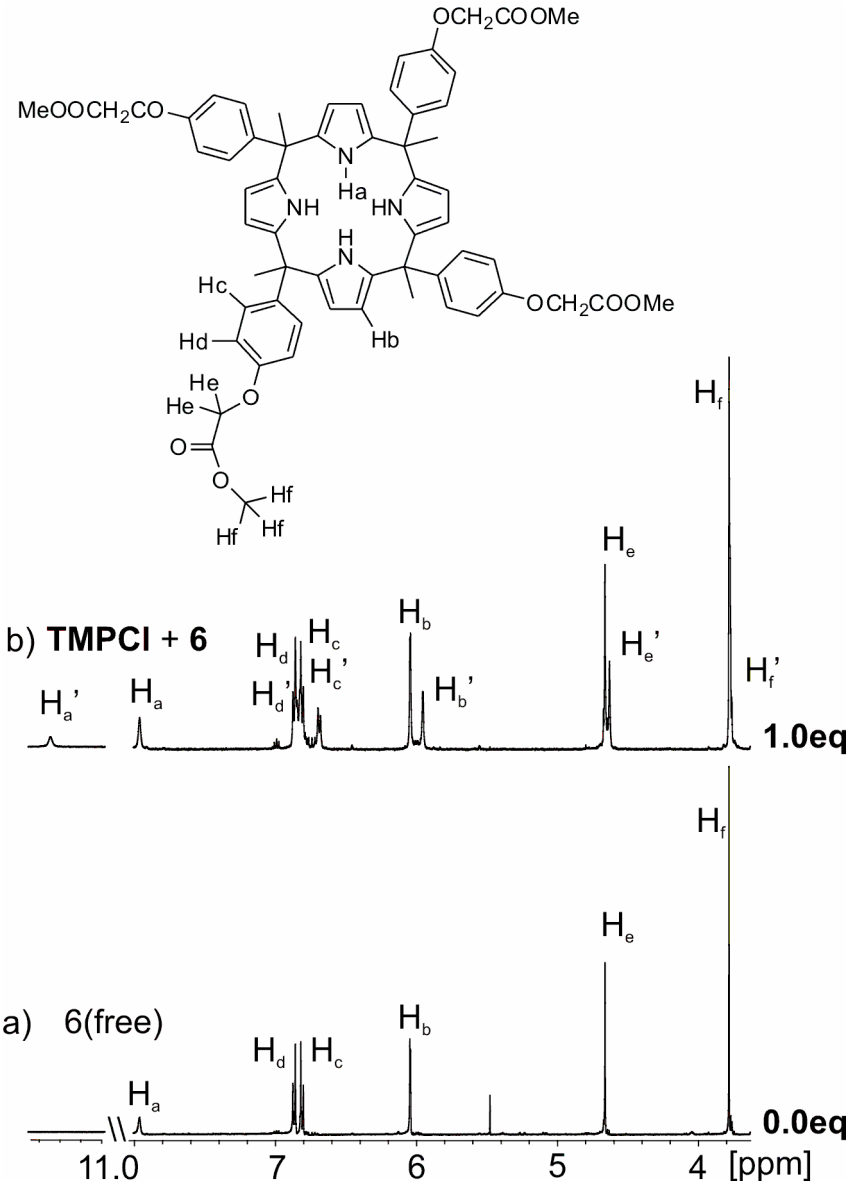

Figure S34. Selected regions of ^{1}H-NMR spectrum of a 3.28mM solution of **6** in ACN-d_3 after the addition of a) 0 equivalents and b) 1.0 equivalent of TMPCl.

10.ESI-MS experiments of 4oo with TMPCl

The MS experiments were carried out using an Electrospray Ionization source combined with a Time-of-Flight mass spectrometer (ESI-TOF), operating in negative and positive mode. The samples were continuously sprayed using nitrogen as drying gas (desolvation at 510 L/hr). The injection rate was maintained constant at 20μL/min. The voltage applied at the ESI needle was increased from 0V to 500V, while a voltage of 0V was applied to the cone. The source and desolvation temperatures were set to 120 ºC and 200 ºC, respectively.

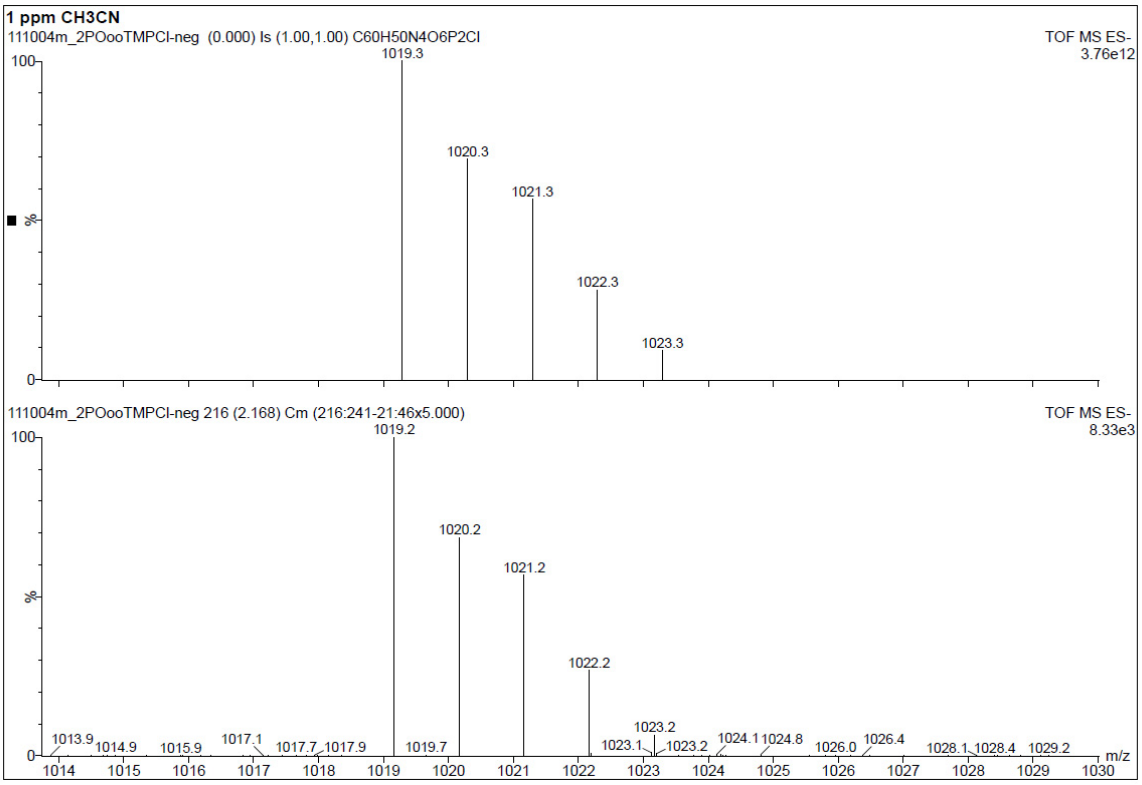

Figure S35. Negative ESI-MS Expansion at 5000V (at the bottom) and calculated isotopic distribution (on the top) for the ion peak with m/z 1019.2 corresponding to the anionic complex **4oo**@Cl^- obtained by spraying a solution containing the **4oo** stereoisomer and TMPCl.

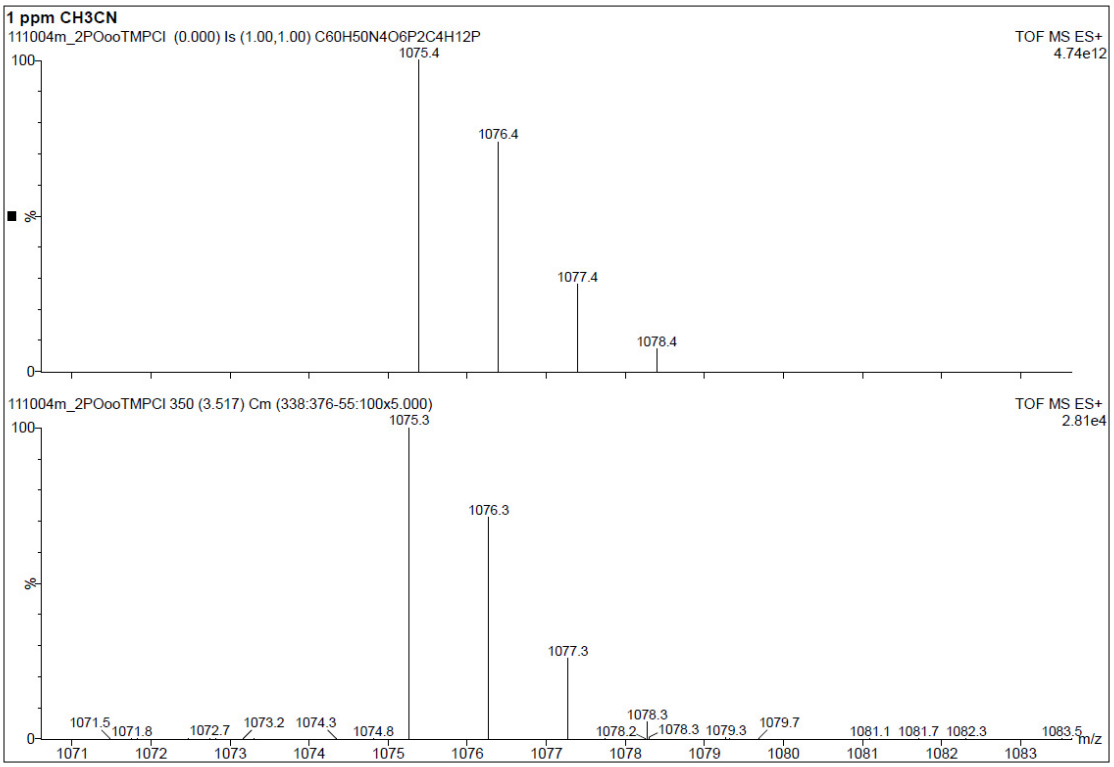

Figure S36. Positive ESI-MS Expansion at 5000V (at the bottom) and calculated isotopic distribution (on the top) for the ion peak with m/z 1075.3 corresponding to the cationic complex **4oo**@TMP^+ obtained by spraying a solution containing the **4oo** stereoisomer and TMPCl.

11.ITC experiments of bis-phosphonate cavitands 4 with TMPCl

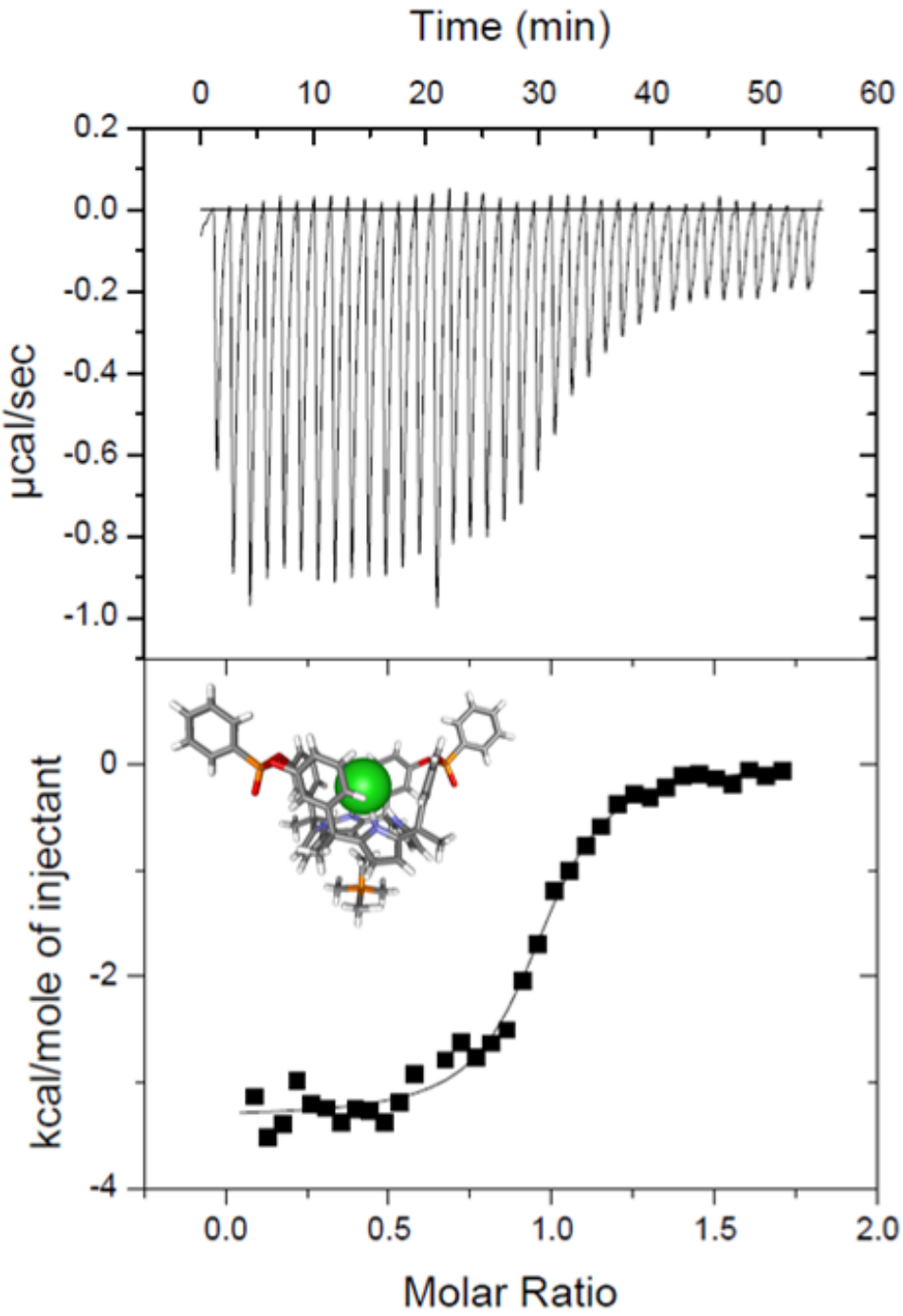

Figure S37. Top: Raw data for the ITC titration of TMPCl into **4oo**. The titration was performed in dichloromethane at 25 ºC. Bottom: Binding isotherm of the calorimetric titration data shown on top. The enthalpy of binding for each injection is plotted against the ratio of concentrations of TMPCl/**4oo**. The continuous line represents the fit of the data to a single-site binding model. $K_{a,exp}$(TMPCl@4oo) = 8 ± 1 × 10^5 M^{-1}; ΔG = – 8.0 kcal/mol; ΔH = – 3.3 kcal/mol; $T\Delta S$ = – 4.7 kcal/mol.

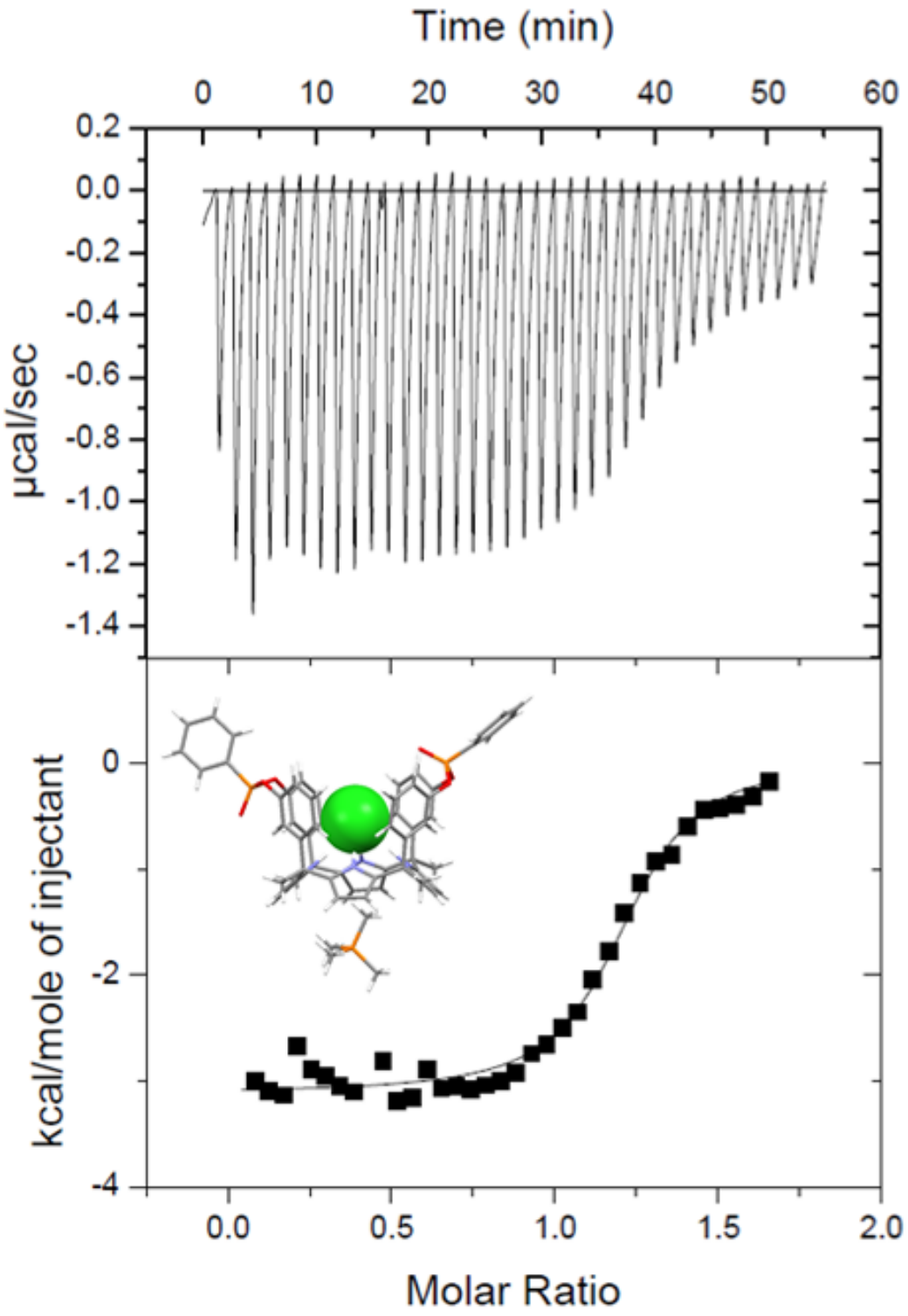

Figure S38. Top: Raw data for the ITC titration of TMPCl into **4io**. The titration was performed in dichloromethane at 25 ºC. Bottom: Binding isotherm of the calorimetric titration data shown on top. The enthalpy of binding for each injection is plotted against the ratio of concentrations of TMPCl/**4io**. The continuous line represents the fit of the data to a single-site binding model. $K_{a,exp}$(TMPCl@4io) = 5 ± 1 × 10^5 M^{-1}; ΔG = – 7.7 kcal/mol; ΔH = – 3.1 kcal/mol; $T\Delta S$ = – 4.6 kcal/mol.

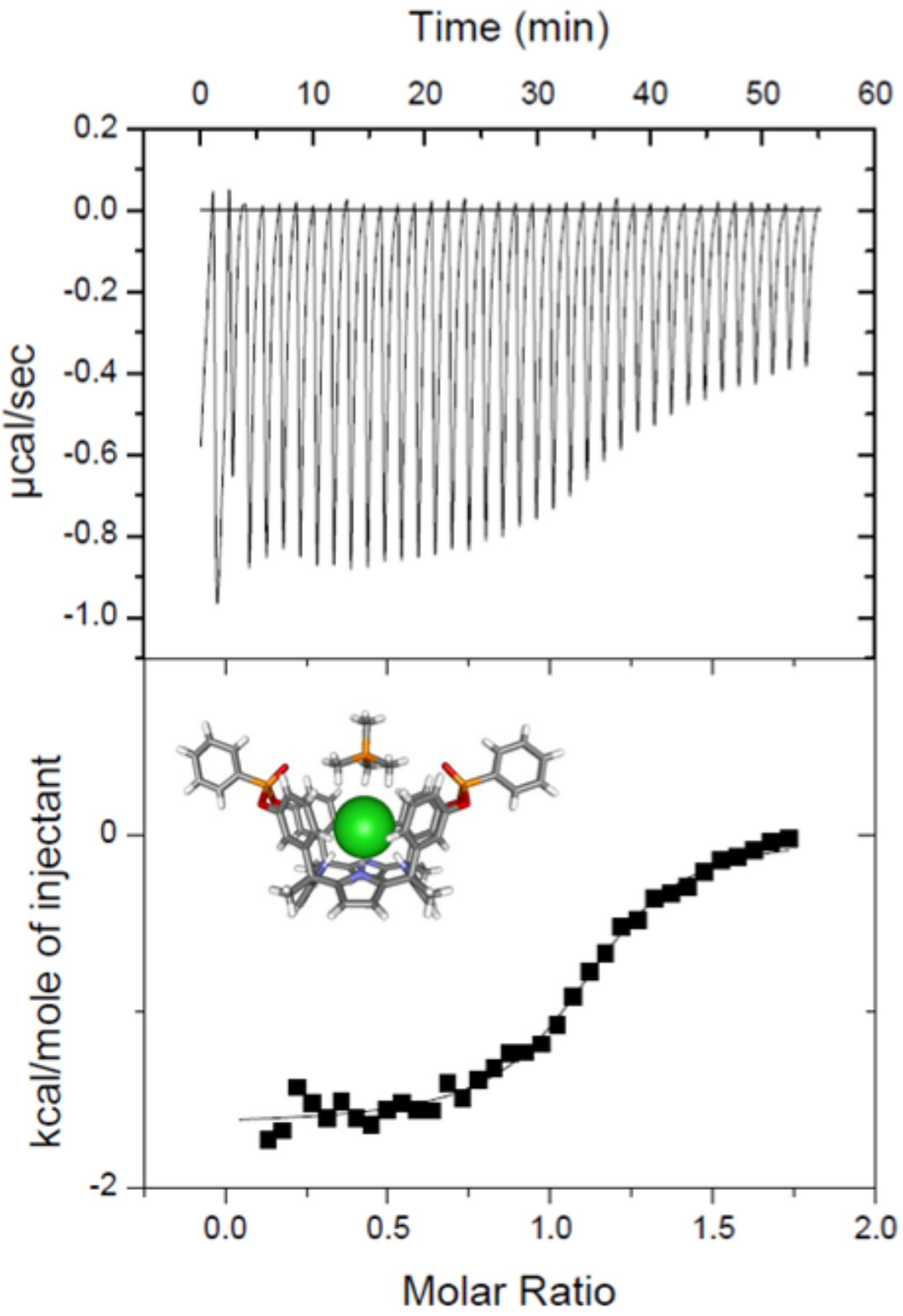

Figure S39. Top: Raw data for the ITC titration of TMPCl into **4ii**. The titration was performed in dichloromethane at 25 ºC. Bottom: Binding isotherm of the calorimetric titration data shown on top. The enthalpy of binding for each injection is plotted against the ratio of concentrations of TMPCl/**4ii**. The continuous line represents the -fit of the data to a single-site binding model. $K_{a,exp}$(TMPCl@4ii) = 2 ± 0.5 × 10^5 M^{-1}; ΔG = – 7.2 kcal/mol; ΔH = – 1.9 kcal/mol; $T\Delta S$ = – 5.3 kcal/mol.

12. Conductimetric Titration

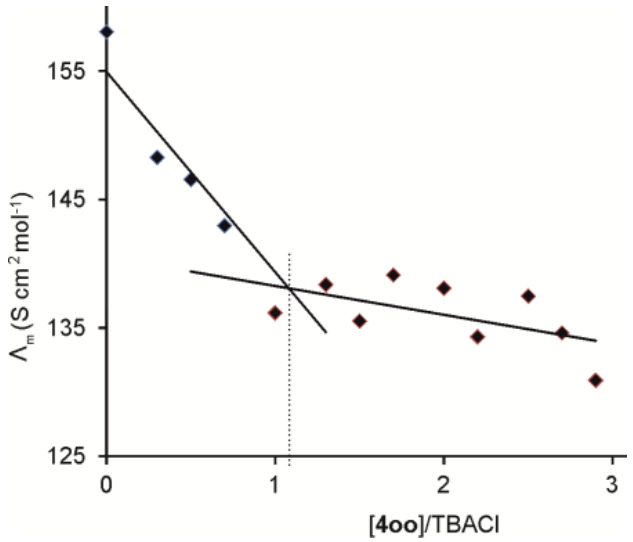

Figure S40. Conductimetric titration curve of chloride anion (TBACl) with **4oo** in ACN solution at 298 K

We performed a conductimetric titration for the pair **4oo** and TBACl in ACN. The plot of molar conductance Λ_m(S cm^2 mol^{-1}), against the receptor/ion concentration ratio [**4oo**]/[Cl$^-$] is shown in Figure S40. The observation of a significant conductance value (158 S cm^2 mol^{-1}) at [**4oo**]/[Cl$^-$] = 0, which is very close to the Λ_m^o value for TBACl in this solvent was a clear indication that the salt was mainly in the form of ionic species.[4] The incremental addition of **4oo** to the ACN solution of [TBACl]= 9.8 × 10^{-5} M^{-1} induced a decrease in the molar conductance. This is due to the complexation of the chloride by the receptor. The volume of the Cl$^-$@**4oo** complex is larger than that of the free chloride. Therefore, the diffusion rate of the complex in solution is reduced compared to that of the free chloride. The conductimetric titration data could be adjusted to two different linear segments that intersect close to the expected value of [**4oo**]/[Cl$^-$] ratio for the formation of a 1:1 complex. This result strongly supports the use of equation (5) in determining the binding affinity constants for receptors **4oo** and **4io** with chloride in ACN solution.

13.X-Ray structural determination

13.1. Experimental

Crystal data and experimental details for data collection and structure refinement are reported in Tables S1 and S2.

The crystal structures of compounds **4ii**, **4oo**, **4io**, TMPCl@**4ii,** TMPCl@**4oo,** TMPCl@**4io** and DTMACl@**4ii** were determined by X-ray diffraction methods. Intensity data and cell parameters were recorded on i) a Bruker AXS Smart 1000 diffractometer (**4ii** and **4io**) and a Bruker APEX II (**4oo**), both equipped with a CCD area detector and a graphite monochromator (MoKα radiation λ = 0.71073 Å); ii) a Bruker-Nonius diffractometer equipped with an APPEX 2 4K CCD area detector, a FR591 rotating anode with MoKα radiation and Montel mirrors (TMPCl@**4ii**, TMPCl@**4io** and DTMACl@**4ii**); iii) a Bruker Kappa APEX II DUO diffractometer equipped with an APPEX 2 4K CCD area detector and a Microsource with MoKα radiation (TMPCl@**4oo**).

The raw frame data were processed using various versions of SAINT and SADABS to yield the reflection data file[5].

The structures were solved by Direct Methods using the SIR97 or SIR2011 programs[6] and refined on F_o^2 by full-matrix least-squares procedures, using the SHELXL-97 or the SHELXTL V6.14 programs[7], the first in the WinGX suite v.1.80.05[8].

The PLATON SQUEEZE procedure[9] was used for compound **4io** to treat regions of diffuse solvent which could not be sensibly modelled in terms of atomic sites. Their contribution to the diffraction pattern was removed and modified F_o^2 written to a new HKL file. The number of electrons located were included in the formula, formula

weight, calculated density, μ and F(000). This residual electron density was assigned to four acetonitrile molecules per unit cell.

All non-hydrogen atoms were refined with anisotropic atomic displacements except in case of disorder or for some of the lattice solvent molecules. The hydrogen atoms were included in the refinement at idealized geometry (C-H 0.95 Å) and refined "riding" on the corresponding parent atoms. The weighting schemes used in the last cycle of refinement were $w = 1/ [\sigma^2 F_o^2 + (0.1217P)^2]$, $w = 1/ [\sigma^2 F_o^2 + (0.1121P)^2]$, $w = 1/ [\sigma^2 F_o^2 + (0.0156P)^2]$, $w = 1/ [\sigma^2 F_o^2 + (0.0501P)^2 + 13.8154P]$, $w = 1/ [\sigma^2 F_o^2 + (0.0599P)^2 + 3.4094P]$, $w = 1/ [\sigma^2 F_o^2 + (0.0785P)^2 + 7.3163P]$ and $w = 1/ [\sigma^2 F_o^2 + (0.1085P)^2 + 1.3987P]$, where $P = (F_o^2 + 2F_c^2)/3$, for **4ii**, **4oo**, **4io**, TMPCl@**4ii,** TMPCl@**4oo,** TMPCl@**4io** and DTMACl@**4ii** respectively. Drawings were obtained using the programs UCFS Chimera and ORTEP[10]

13.2. Tables

Table S1. Crystal data and structure refinement information for compounds **4ii**, **4oo**, **4io**.

Compound	**4ii**	**4oo**	**4io**
Formula	$C_{62}H_{57}N_5O_8P_2$	$C_{64}H_{56}N_6O_6P_2$	$C_{73}H_{67}N_9O_7P_2$
FW	1062.07	1067.09	1244.30
Crystal system	Orthorhombic	Orthorhombic	Triclinic
Space group	*Pnma*	$P2_12_12_1$	*P-1*
a (Å)	11.097(3)	16.273(2)	10.994(2)
b (Å)	21.896(6)	17.888(2)	13.654(2)
c (Å)	22.955(6)	19.236	22.642(3)
α (º)	-	-	88.100(3)
β (º)	-	-	79.105(3)
γ (º)	-	-	76.970(3)
V (Å^3)	5578(3)	5599(1)	3251.4(9)
Z	4	4	2
T (K)	293(2)	293(2)	190(2)
ρ (g cm^{-3})	1.265	1.266	1.271
μ (mm^{-1})	0.138	0.136	0.129
F(000)	2232	2240	1308
Total reflections	13748	36839	38993
Unique reflections (R_{int})	7153 (0.0598)	13752 (0.0949)	14136 (0.1022)
Observed reflections [$F_o>4\sigma(F_o)$]	2593	5696	4340

GOF on F^{2a}	1.004	0.993	0.984
R indices $[F_o>4\sigma(F_o)]^b$ R_1, wR_2	0.0891, 0.2251	0.0808, 0.1945	0.0642, 0.0989
Largest diff. peak and hole ($eÅ^{-3}$)	1.379, -0.289	0.872, -0.360	0.487, -0.352

aGoodness-of-fit $S = [\Sigma w(F_o^2-F_c^2)^2/ (n-p)]1/2$, where n is the number of reflections and p the number of parameters. $^bR_1 = \Sigma \| F_o | - | F_c \| / \Sigma | F_o |$, $wR_2 = [\Sigma[w(F_o^2-F_c^2)^2]/\Sigma[w(F_o^2)^2]]^{1/2}$.

Table S2. Crystal data and structure refinement information for compounds TMPCl@**4ii**, TMPCl@**4oo**, TMPCl@**4io**, DTMACl@**4ii**.

Compound	TMPCl@**4ii**	TMPCl@**4oo**	TMPCl@**4io**	DTMACl@**4ii**
Formula	$C_{65}H_{64}Cl_3N_4O_6P_3$	$C_{65}H_{64}Cl_3N_4O_6P_3$	$C_{66}H_{66}Cl_5N_4O_6P_3$	$C_{77}H_{87}Cl_5N_5O_6P_2$
FW	1196.46	1196.46	1281.39	1417.71
Crystal system	Monoclinic	Monoclinic	Monoclinic	Monoclinic
Space group	*P21/c*	*P21/c*	*P21/n*	*P21/n*
a (Å)	12.646(1)	16.784(1)	16.4602(5)	18.038(1)
b (Å)	20.498(2)	18.076(1)	19.4188(6)	22.494(1)
c (Å)	23.256(2)	20.025(1)	21.0109(7)	18.810(1)
β (º)	91.325(5)	99.529(3)	111.798(2)	110.227(3)
V ($Å^3$)	6027(1)	5991.4(6)	6235.7(3)	7161.1(8)
Z	4	4	4	4
T (K)	100(2)	100(2)	100(2)	100(2)
ρ (g cm^{-3})	1.319	1.326	1.365	1.315
μ (mm^{-1})	0.287	0.289	0.365	0.304
F(000)	2504	2504	2672	2988
Total reflections	76379	46009	172527	41220
Unique reflections (R_{int})	7401 (0.0881)	13274 (0.0470)	21877 (0.0502)	7506 (0.1487)
Observed reflections [$F_o>4\sigma(F_o)$]	5738	9408	17231	4178
GOF on F^{2a}	1.100	1.035	1.044	1.018
R indices [$F_o>4\sigma(F_o)$]^b R_1, wR_2	0.0535, 0.1288	0.0453, 0.1104	0.0575, 0.1556	0.0713, 0.1676

Largest diff. peak and hole ($eÅ^{-3}$)	0.919, -0.441	0.569, -0.580	0.736, -0.846	0.667, -0.576

[a]Goodness-of-fit S = $[\Sigma w(F_o^2-F_c^2)^2/ (n-p)]1/2$, where n is the number of reflections and p the number of parameters. [b]$R_1 = \Sigma \| F_o | - | F_c \| / \Sigma | F_o |$, $wR_2 = [\Sigma[w(F_o^2-F_c^2)^2]/\Sigma[w(F_o^2)^2]]^{1/2}$.

13.3. Ortep views

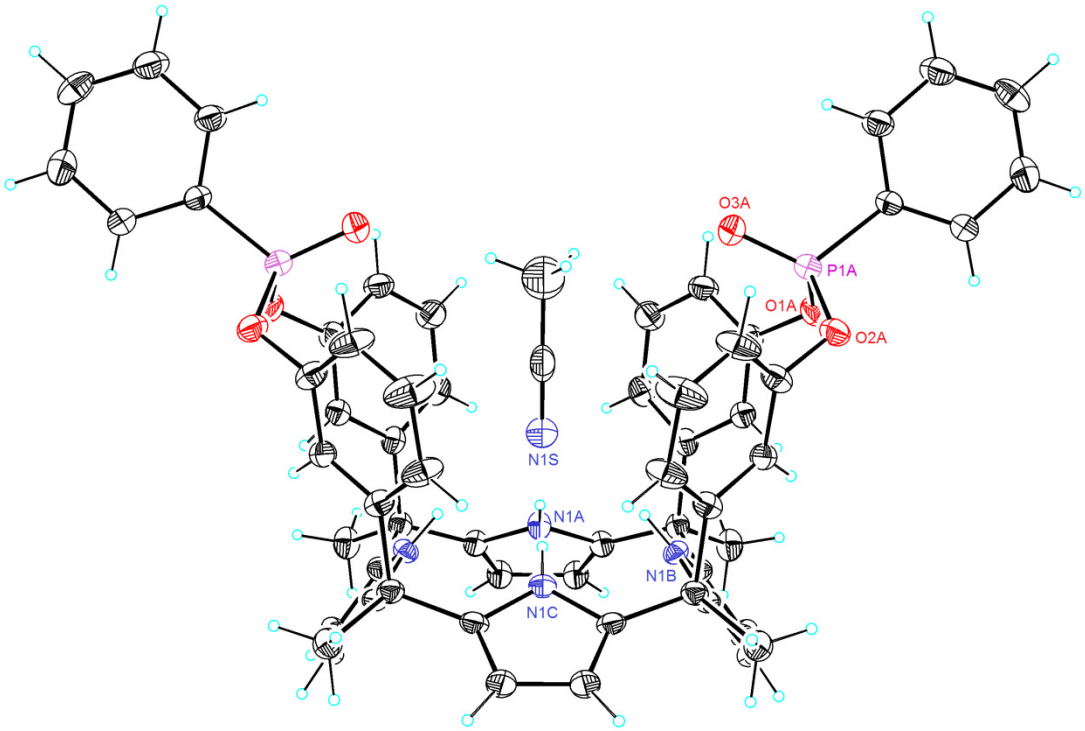

Figure S39. Ortep view of **4ii** (lattice solvent molecules have been omitted)

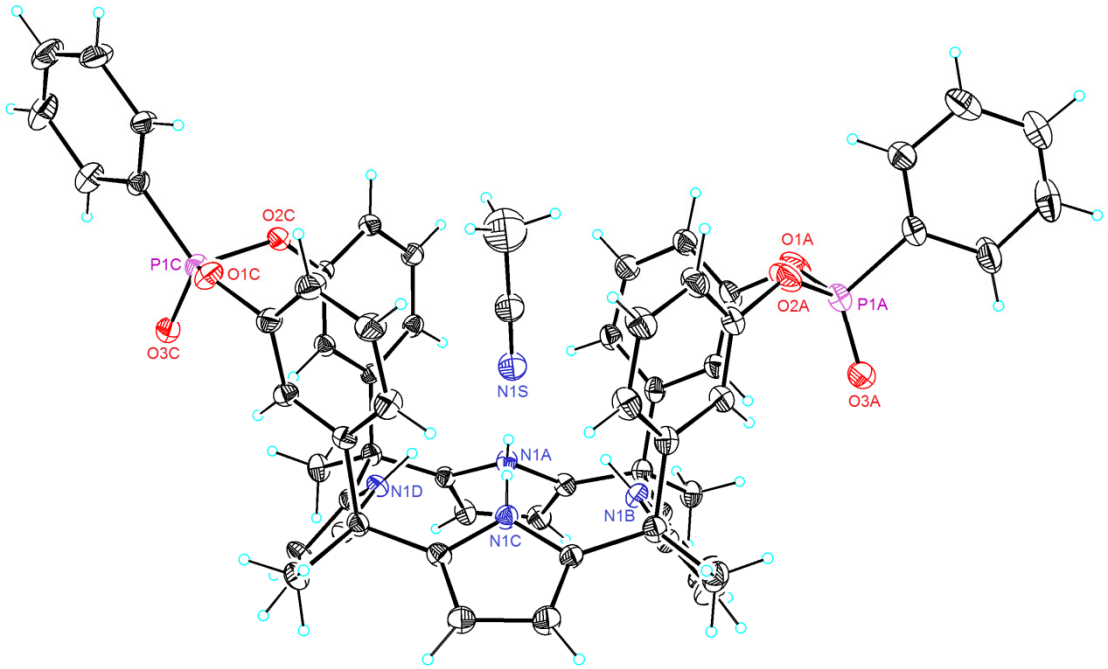

Figure S40. Ortep view of **4oo** (lattice solvent molecules have been omitted)

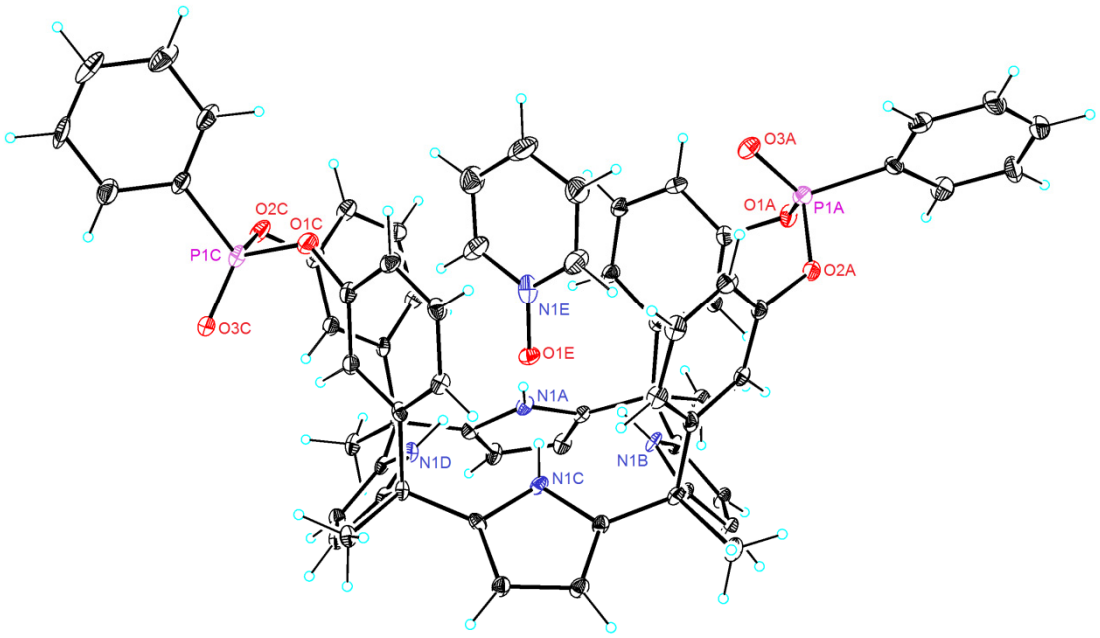

Figure S41. Ortep view of **4io** (lattice water molecules have been omitted).

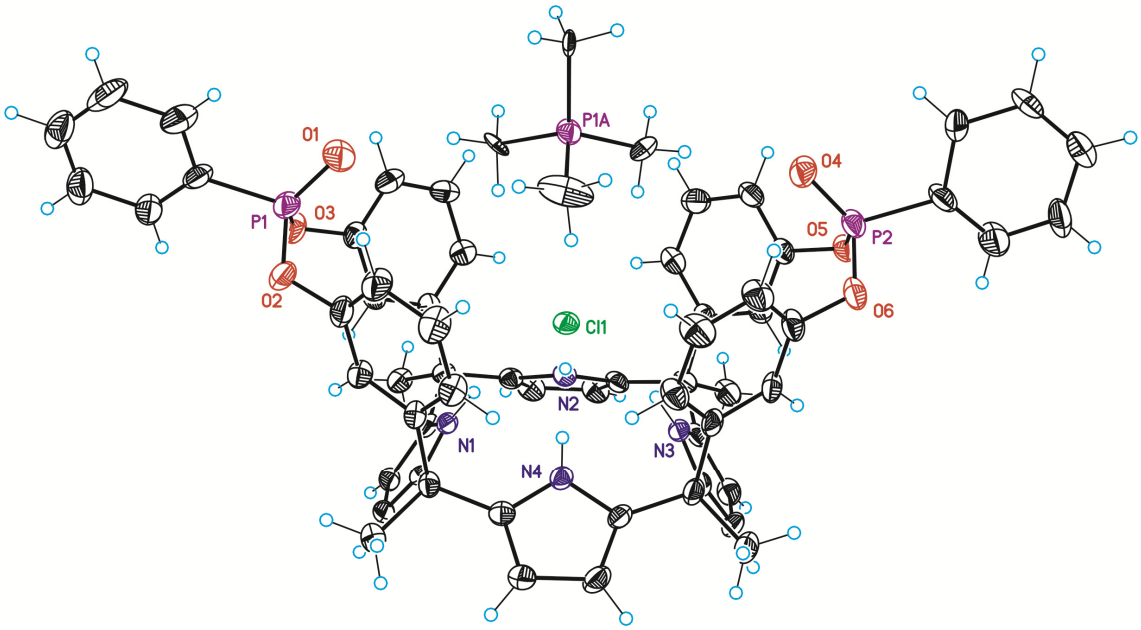

Figure S42. Ortep view of TMPCl@**4ii** (lattice solvent molecules have been omitted).

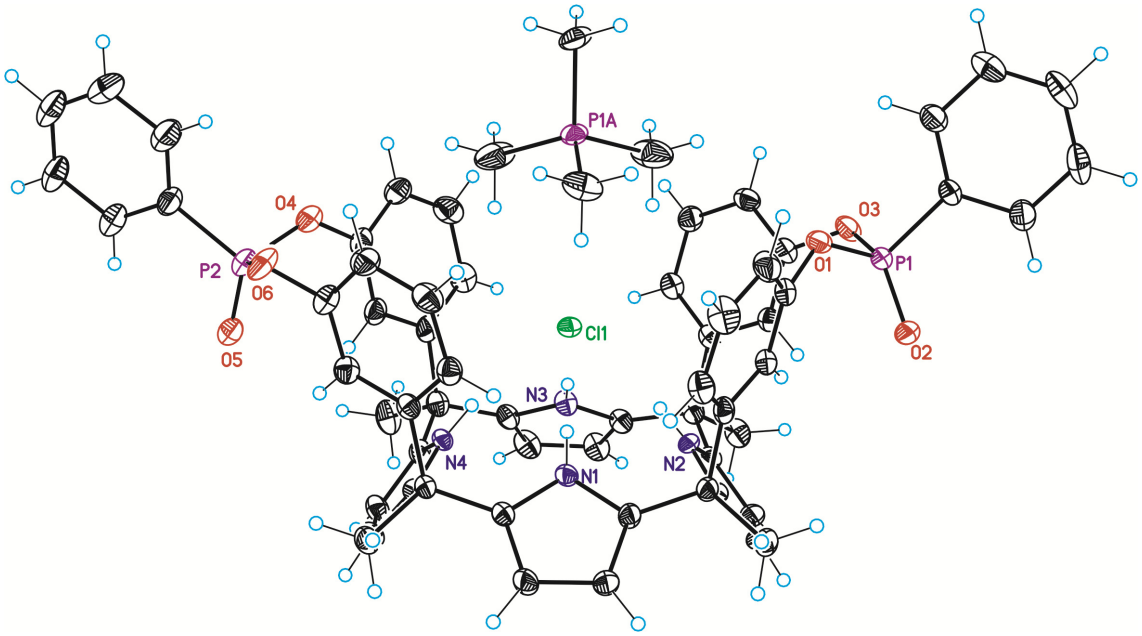

Figure S43. Ortep view of TMPCl@**4oo** (lattice solvent molecules have been omitted).

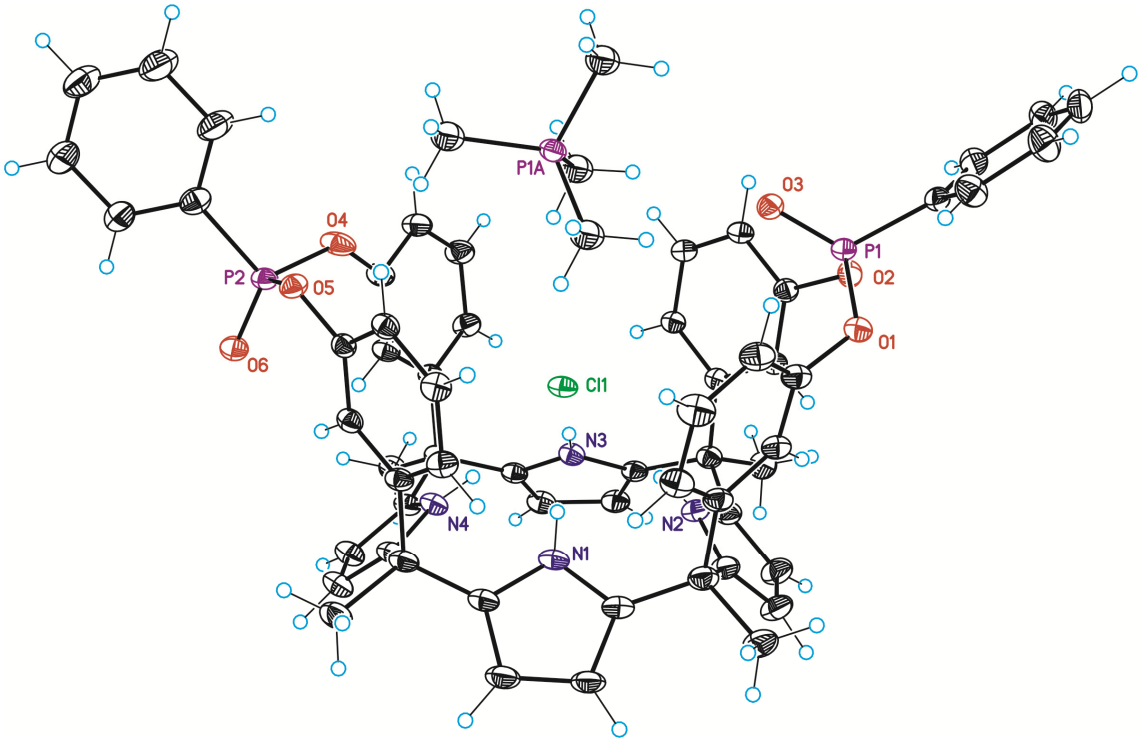

Figure S44. Ortep view of TMPCl@**4io** (lattice solvent molecules have been omitted).

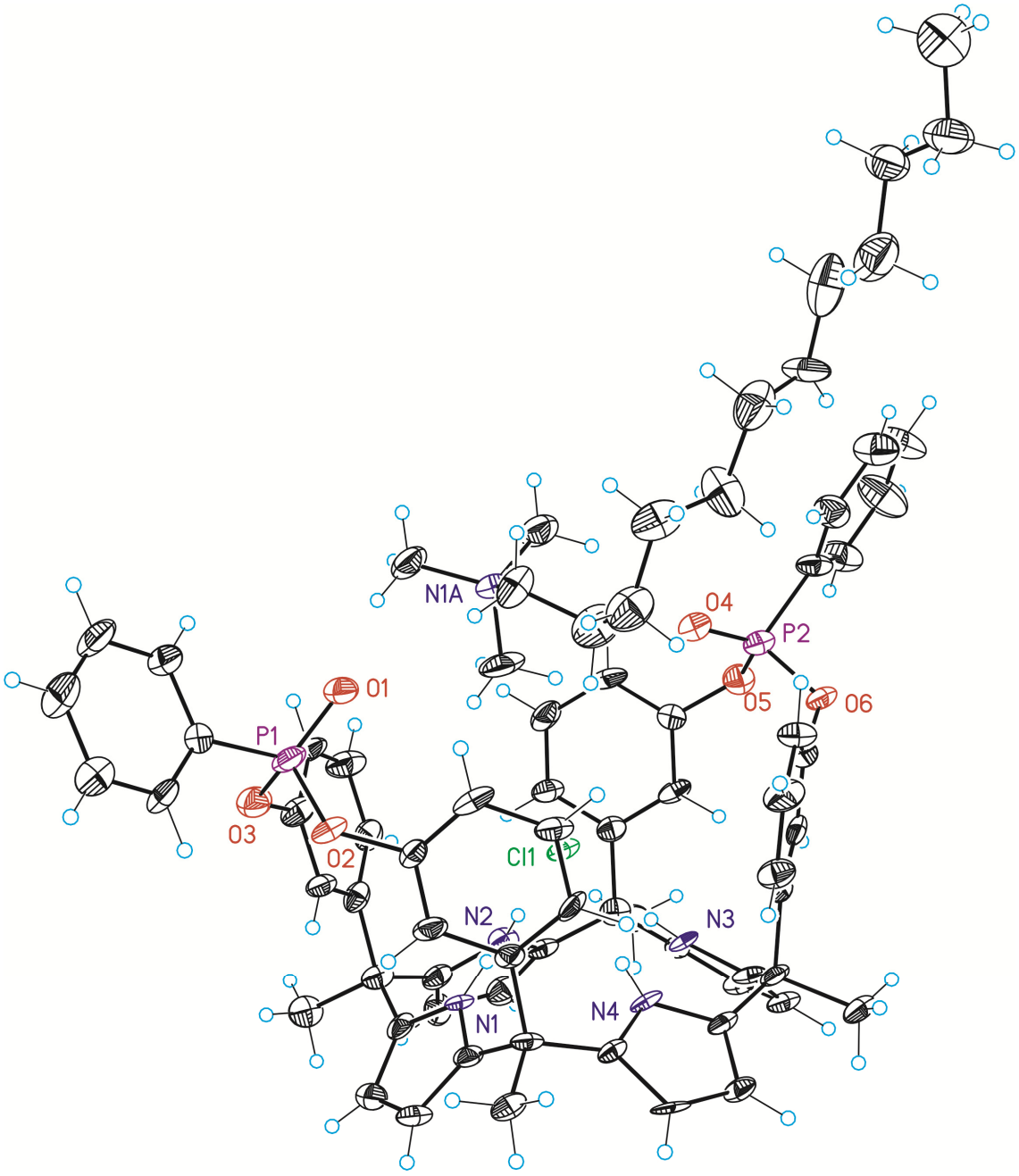

Figure S45. Ortep view of DTMACl@**4ii**#lattice solvent molecules have been omitted).

13.4. Columnar Packing motif in the crystal of the DTMACl@4ii Complex.

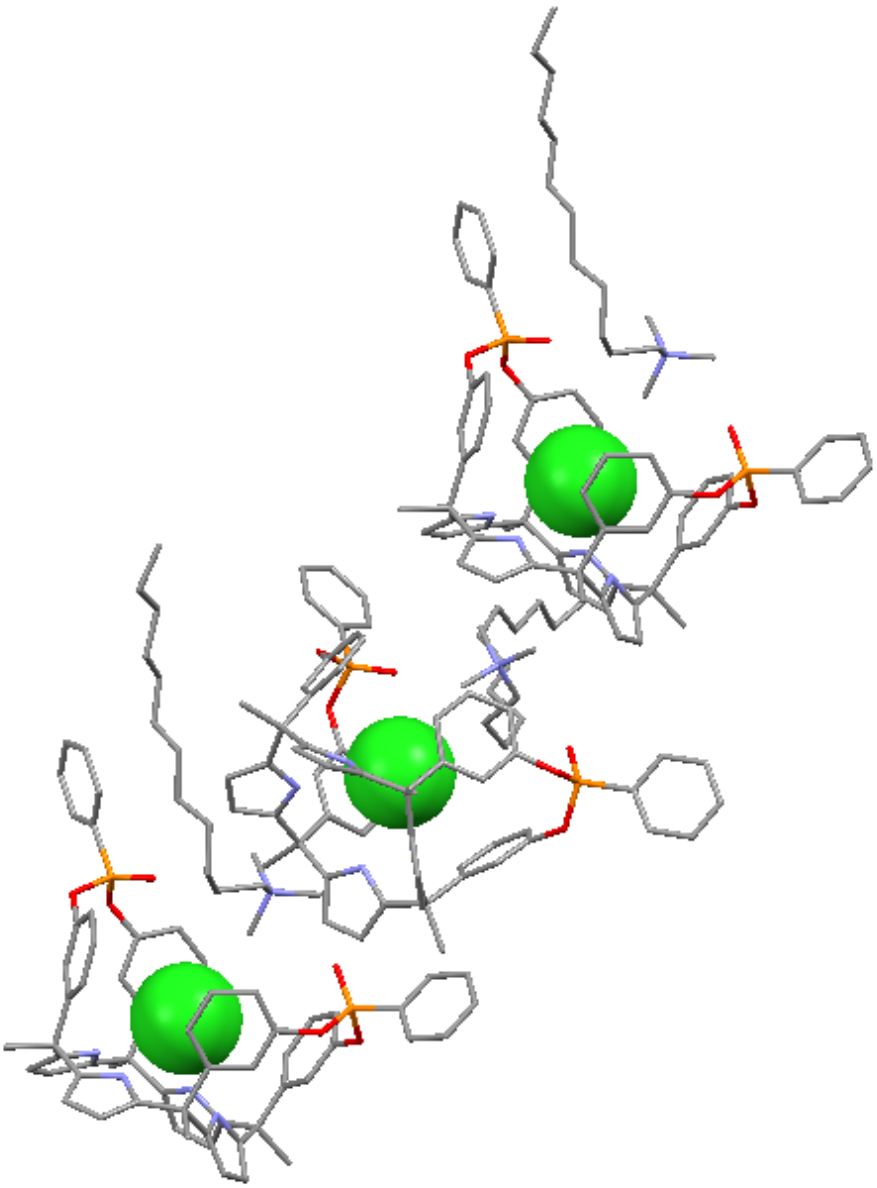

13.5. Columnar Packing motifs in the Crystals of the Methyl-Pyridinium@4 Complexes

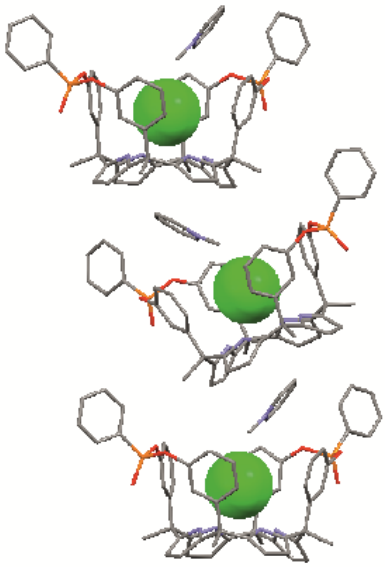

MePyr@**4oo**

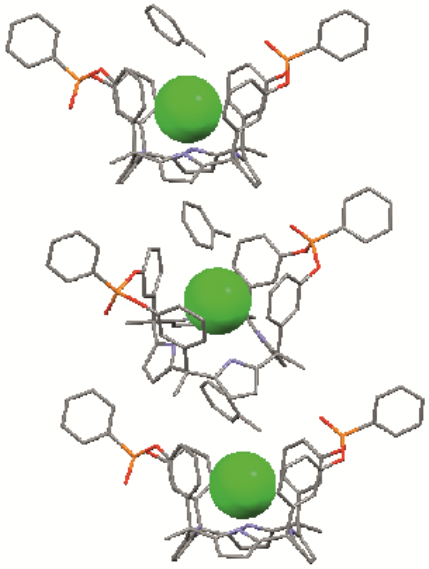

MePyr@**4io**

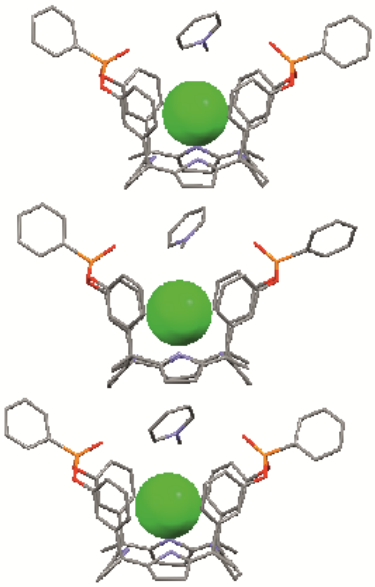

MePyr@**4ii**

(1) Bonomo, L; Solari, E; Toraman, G. Scopelliti, R.; Latronico, M.; Floriani, C. *Chem. Commun.* **1999**, 2413-2414.

(2) a) Yebeutchou, R. M.; Tancini, F.; Demitri, N.; Geremia, S.; Mendichi, R.; Dalcanale, E., *Angew. Chem., Int. Ed.*, **2008**, *47*, 4504-4508, b) Tancini, F.; Yebeutchou, R. M.; Pirondini, L.; De Zorzi, R.; Geremia, S.; Scherman, O. A.; Dalcanale, E., *Chem. Eur. J.*, **2010**, *16*, 14313-14321.

(3) Camiolo, S.; Gale, P. A. *Chem. Commun*. **2000**, 1129-1130.

(4) de Namor, A. F. D.; Khalife, R., *Phys. Chem. Chem. Phys.*, **2010**, *12*, 753-760.

(5) SADABS Bruker AXS; Madison, Wisconsin, USA, 2004; SAINT, *Software Users Guide*, *Version 6.0*; Bruker Analytical X-ray Systems, Madison, WI, **1999**. Sheldrick, G. M. SADABS v2.03: *Area-Detector Absorption Correction*. University of Göttingen, Germany, **1999**; Saint + Version 7.60A (Bruker AXS 2008); SADABS V. 2008-1 (2008).

(6) a) Altomare, A.; Burla, M. C.; Camalli, M.; Cascarano, G. L.; Giacovazzo, C.; Guagliardi, A.; Moliterni, A. G. G.; Polidori, G.; Spagna, R. *J. Appl. Crystallogr*. **1999**, *32*, 115; b) SIR2011: Burla, M. C; Caliandro, R.; Camalli, M.; Carrozzini, B.; Cascarano, G. L.; Giacovazzo, C.; Mallamo, M.; Polidori, G.; Spagna, R.

(7) Sheldrick, G. M. *SHELXL-97. Program for Crystal Structure Refinement*. University of Göttingen, Germany, **1997** and *Acta Crystallogr*. **2008**, *A64*, 112.

(8) Farrugia, L. J., *J. Appl. Crystallogr*., **1999**, *32*, 837-838.

(9) *SQUEEZE* - v.d Sluis, P.; Spek, A. L. *Acta Crystallogr., Sect A* **1990**, *46*, 194.

(10) a) UCSF Chimera--a visualization system for exploratory research and analysis. Pettersen E. F.; Goddard T. D.; Huang C. C.; Couch G. S.; Greenblatt D. M.; Meng E. C; Ferrin T. E. *J Comput Chem.* **2004**, *25*, 1605-12; b) Ortep-3 for windows in the WinGX suite. Farrugia, L. J., *J. Appl. Crystallogr*., **1997**, *30*, 565.